Bending Characteristics of Carbon Nanotubes: Micropolar Elasticity Models and Molecular Dynamics Simulations

Razie Izadi[1], Meral Tuna[2], Patrizia Trovalusci[1,*], and Nicholas Fantuzzi[3]

[1]*Department of Structural and Geotechnical Engineering, Sapienza University of Rome, Via A. Gramsci, 53, 00197 Rome, Italy;razie.izadi@uniroma1.it*
[2]*Faculty of Engineering, Yaşar University, Universite Caddesi, Agacli Yol, 37-39, Izmir 35100, Turkey; meral.tunaeroglu@yasar.edu.tr*
[3]*Department of Civil, Chemical, Environmental and Materials Engineering, University of Bologna, Viale del Risorgimento 2, Bologna 40136, Italy; nicholas.fantuzzi@unibo.it*
[*]*Correspondence: patrizia.trovalusci@uniroma1.it*

September 2021

Bending Characteristics of Carbon Nanotubes: Micropolar Elasticity Models and Molecular Dynamics Simulations

Abstract

The present paper aims at evaluating non-classical continuum parameters for each class of armchair and zigzag single-walled CNTs focusing on the scale effect in their flexural behavior observed in molecular dynamics (MD) simulations. Through a non-linear optimization approach, the bending rigidities obtained from atomistic simulations are compared to those derived from non-classical continua. For MD simulations, a novel method ensuring pure bending is introduced and for continuum modeling, micropolar, constrained micropolar, and modified couple stress theories are employed. The results reveal that adopted non-classical theories, notably micropolar theory, provide reasonable outcomes with an obvious failure of classical Cauchy theory.

keywords:micropolar continua; molecular dynamics simulation; size effect in bending modulus; SWCNTs parameters identification; optimization

1 Introduction

1.1 *Applications and Literature Review*

Carbon nanotubes (CNTs) [1, 2] have many actual and potential applications in different fields of engineering (e.g. sensors [3], actuators [4, 5], springs [6], resonators [7, 8], reinforcement elements [9–12], probes [13–16]) thanks to their outstanding mechanical, optical, thermal and electrical properties [17–20]. Even though discrete modeling techniques can precisely mimic the response of the corresponding media with a proper choice of interatomic potential and realistic boundary/loading conditions [21–26] [27–30], limitations are imposed both on time and scale of the problem due to computational concerns [31], while experimental methods might suffer from physical challenges (e.g. sample preparation/handling, analysis, data extraction) [32, 33].

Among various efforts that have been made to describe the behavior of nanostructures (including CNTs), continuum models that are evaluated in accordance with findings of atomistic simulations or actual experiments, may well be used to reduce the computational burden by approximating corpuscular structures with continuous functions [34–36]. The simplest continuum model to be resorted is the classical Cauchy of grade 1, yet it suffers from limitations of not being able to contain information about internal size, strain asymmetries and particle orientations [34, 37], which can be considered as the source of scale effects in CNTs [33, 38–42]. These drawbacks can be overcome with the aid of non-classical (non-local) continuum theories that utilize field description at coarse level and preserve the memory of material's underlying structure at fine level through internal scale parameters [43–48]. As suggested by Kunin [49], Maugin [50] and Eringen [47], a distinction between 'explicit'/'strong' and 'implicit'/'weak' non-local formulations can be made depending on the kind of non-locality. This classification was first adopted by Trovalusci [34], and further by other studies [51–54]. In the so-called explicit type non-local models, such as Eringen's

model [55], primal fields of classical theory is preserved while equations of motion contain integral, integro-differential or finite-difference operators in the spatial field to cover the long-range interactions through non-local parameter [48, 56]. On the other hand, in implicit type non-local theories, also referred to microcontinuum field theories or multi-field continua [47], each material point is endowed with additional degrees of freedom (DOF) that can account for size effects. In micropolar theory, as a subset of microcontinuum field theories, this non-standard DOF is set to be the microrotation and consequently additional strain and stress measures as well as material parameters containing information about internal structure are introduced into the field and constitutive equations [49, 50, 57, 58]. As a result, micropolar theory has been successfully used to describe a wide range of materials with internal structures, especially those where relative rotations are predominant, such as brick masonry-like materials [59–61], heterogeneous structures with internal cracks/voids/inclusions [62–65], and particulate composites [66–70]. A subcase of micropolar theory is the couple stress theory originally developed by Toupin [71], Mindlin and Tiersten [72] and Koiter [73], in which microrotations are constrained to follow macrorotations (local rigid rotations) yielding symmetric strain measures [74, 75], however, it should be noted that the original form of couple stress theory suffers from indeterminacy of the spherical part of couple stress tensor and the appearance of the normal component of couple traction vector on boundary surfaces [47, 76, 77]. To overcome this inconsistency, different versions of couple stress theory have been developed. Yang et al. proposed modified couple stress theory [78] in which the microrotations still equals the macrorotation while the strain energy is assumed to depend only on the symmetric part of the strain and curvature tensors, providing a symmetric couple stress tensor and only one additional length scale parameter besides classical material constants. Due to the greater simplicity of size-dependent modified couple stress theory than micropolar theory and original couple stress theory, it is frequently adopted to study the mechanical behavior of size-dependent materials and nanostructures [79–83], although there still exists some criticism on this theory regarding ill-posed boundary conditions [77].

A number of studies have addressed the size-dependent behavior of single-walled and multi-walled carbon nanotubes through static analysis like flexural and torsional deformation and buckling [84–86] and dynamic analysis like free vibration and wave propagation [87–90]. The occurrence of size effect is due to the fact that at nano-scales, the lattice spacing between individual atoms is comparable to the overall dimensions (e.g., length, diameter) and the discrete nature of the underlying material organization affects the gross mechanical behavior of the structure. As classical theory cannot capture the size dependency, non-local theories, which can include the effect of material length scales, are often recommended when continuum modeling is desired. A review on the subject is provided in [91], while as one can see the majority utilizes explicit type non-local theories [92–97]. All these considered, investigating the capacity of the implicitly non-local micropolar and couple stress theories on describing the overall behaviour of CNTs is tempting as there exist limited number of studies on the subject. So far, few studies have adopted micropolar theory to model CNTs. For instance, Xie and Long [98] calculated the fundamental frequencies of single and double-walled CNTs using the concept of micropolar elasticity. However, the application of couple stress theory in CNT modeling is more common than micropolar theory;

Akgoz and Civalek [83] adopted modified couple stress theory and Euler-Bernoulli beam model to calculate the critical axial compressive buckling loads of CNTs. Khajueenejad and Ghanbari [82] estimated variable internal length parameters for zigzag and armchair CNTs using modified couple stress Timoshenko beam theory and the axial buckling loads from molecular dynamics (MD) simulations. Fakhrabadi et al. [42], used modified couple stress theory with average material parameters of CNTs to show size-dependent mechanical behaviors of the cantilever and doubly clamped CNTs under electrostatic actuation. Khorshidi [41] used a modified couple stress Timoshenko beam with the weakening effect to capture the fall in the phase velocity curve vs the wave number observed in the MD simulation. They have used MD result for two armchair CNTs found in a study by Wang and Hu [99], and reported different material length scale parameters for each. Farokhi et al [87] developed a size-dependent continuum model based on modified couple stress theory for analysis of the behaviour of carbon nanotube-based resonators. The model is then parameterized and validated employing molecular dynamics simulations. Finally, in a recent contribution of some of the Authors [100], size-dependent behavior of CNTs under torsion is investigated on the basis of micropolar theory, and corresponding material parameter sets of armchair and zigzag CNTs are determined by comparing the difference between the apparent shear modulus obtained from MD simulations and one-dimensional micropolar beam model.

1.2 *Contributions of the Present Study*

With this motivation, in the present study, the applicability of micropolar theory in modeling size-dependent behaviour of CNTs is checked focusing on flexural characteristics. For this purpose, first, a series of MD simulations are performed on armchair and zigzag nanotubes under pure bending, which is ensured by proposing a systematic method that avoids previously reported spurious axial deformations [101–105]. For the sake of computational cost, the length of the CNTs are adjusted to keep the aspect ratio constant at a moderately small value since bending stiffness is proved to be independent of the slenderness. In consistent with experimental observations [106] and atomistic simulations [85], the variation of bending modulus with diameter reveals the existence of size effect, and, indeed, calls for the use of non-local continuum theories to be able to maintain the accuracy of atomistic simulations. For the identification of the corresponding constitutive material parameters, a non-linear optimization approach that aims to reproduce bending rigidities obtained from MD simulations by continuum model is adopted. Here CNTs are considered as three-dimensional hollow cylindrical beams made of homogeneous, isotropic, linear, elastic material. As the exact solution to the bending problem of a micropolar hollow cylinder is rather sophisticated, in the present work the problem is also solved in the framework of modified couple stress theory [78], and constrained micropolar theory, in which the displacement field is assumed to be equal to the classical elastic one and microrotations are enforced to follow the macrorotations [107]. It should be mentioned that the constrained micropolar theory can still account for the asymmetries in the curvature and couple stress fields on the contrary to the modified couple stress theory. The suitability of the two latter theories is then compared with the solution of micropolar theory. To the best of the

Authors' knowledge, this is the first time that micropolar/modified couple stress theory is used to model the size-dependent behavior of CNTs captured in the atomistic simulated bending of CNTs.

The paper is organised as follows; Section 2 describes the details of MD simulation for the pure bending of CNTs by validating and discussing the results. Section 3 addresses the governing equations and derives corresponding bending rigidity expressions for micropolar, constrained micropolar and modified couple-stress theories. In Section 4, the constitutive parameters for each implicit non-local continuum model are determined using a non-linear optimization approach by providing a discussion of the results. Finally, concluding remarks are summarised in Section 5.

2 Atomistic Simulation

Single-walled carbon nanotubes (SWCNTs) can be described as a single layer of graphene sheet rolled into a seamless hollow cylinder with a constant mean diameter. Depending on the direction of wrapping, nanotubes are categorised as armchair ($m = n$), zigzag ($n = 0$) and chiral ($m \neq n$):

$$\mathbf{C}_h = m\mathbf{a}_1 + n\mathbf{a}_2 = (m, n) \tag{1}$$

where $\mathbf{C}_h$ refers to chiral vector, and is specified by chiral index (m, n), alongside with basis vectors of graphene lattice $\mathbf{a}_1$ and $\mathbf{a}_2$ [108].

This section presents the details of MD simulations to perform bending on two sets of eight armchair and zigzag SWCNTs with mean diameters ranging from $d = 6.3 - 16.2$ Å (1 Å = 10^{-10} m), while the aspect ratio, L_0/d which is the ratio of CNTs' free length to the mean diameter, is fixed at a moderately small value ($L_0/d \approx 5$), for the sake of computational cost, however, the independence of bending rigidity to the aspect ratio, which is the output to be implemented in the optimization process in Section 4, is going to be ensured in Section 2.2 The MD simulations are carried out in Large-scale Atomic/Molecular Massively Parallel Simulator (LAMMPS) open-source package [109] using Visual Molecular Dynamics (VMD) software for the visualization [110]. Adaptive intermolecular reactive empirical bond order (AIREBO) potential [111] with a cut-off radius of 10.2 Å is adopted to describe the interatomic interactions, which is a sum of pairwise interactions, including covalent bonding interactions, Lennard–Jones terms, and torsion interactions and one of the most accurate potentials for modelling carbon atoms. Fixed type boundary conditions are considered in three directions. First, each CNT undergoes an energy minimization using the conjugate gradient method, then the structures are relaxed at 10 K (Kelvin) through a canonical (NVT) ensemble where total number of atoms, volume of simulation box and temperature of the system are kept constant [109] with the aid of Nose-Hoover thermostat for 200 picosecond (1 pico = 10^{-12}). The velocity-Verlet algorithm is used for time integration with a step of 1 femto second(1 femto = 10^{-15}). The relatively low temperature is used to eliminate the effect of thermal fluctuations on the mechanical response of CNTs. In order to ensure the independence of the bending rigidity from the aspect ratio and environmental temperature, a series of simulations are performed

considering slender CNTs ($L_0/d = 10, 12, 20$) as well as higher temperature values (300 K).

2.1 *Simulation of Pure Bending*

To apply a loading that resembles pure bending, most researchers keep the end atoms of the CNT frozen while imposing rotation. However, this protocol might create spurious axial strain, and care must be taken to avoid it. Although, there is no distinct consensus on how to prevent it, some researchers like Cao and Chen [103] and Kutana and Giapis [104] have reported to apply displacement besides rotation to remove the effect of spurious axial strain without providing any further details, and Nikiforov [105] has suggested to use the objective MD method instead of MD to avoid the axial forces, while others mentioned nothing regarding the issue. (A summary of different loading methods in the literature is provided in the Appendix.) In the present work, to ensure the pure bending on CNTs, the following procedure is suggested.

1) At the beginning of each increment, a small rotation of 0.003 rad $\simeq 0.17\ ^\circ$ is applied on the boundary atoms at the ends, marked with blue colour (Fig. 1). It should be noted that, boundary atoms do not contribute to the overall (free) length of the nanotube, L_0. The span of boundary atoms at each end, l_{fixed}, is arranged to be in accordance with the overall length of the nanotube, such that the ratio in-between remains constant, (i.e., $l_{fixed}/L_0 \approx 25\%$), however, for CNT(7,7), results are checked to be independent of the span of fixed atoms. The rotation at each side takes place around a line perpendicular to the CNT's axis and passing through the centre of mass of the red ring in Fig. 1. ***[Fig. 1 should be here.]***

2) To keep the length of the deformed CNT axis unaltered, the two ends are moved in the z-axis so that the arc length remains equal to the initial length of the tube, L_0 (Fig. 1). Accordingly, if α_1, ρ_1 and l_1 are the rotation angle, the radius of curvature and end-to-end distance at the beginning of each increment and α_2, ρ_2 and l_2 are their counterparts at the end of the increment (shown schematically in Fig.1), following relation must hold to keep the tube length constant:

$$\rho_1\,(2\alpha_1) = \rho_2\,(2\alpha_2) = L_0 \tag{2}$$

Also, it is evident from Fig. 1 that:

$$\begin{aligned} l_1 &= 2\rho_1 sin\alpha_1 \\ l_2 &= 2\rho_2 sin\alpha_2 \end{aligned} \tag{3}$$

Accordingly, after each rotation the ends should be displaced toward each other for a value of Δl:

$$\Delta l = \frac{1}{2}(l_1 - l_2) = \frac{1}{2}L_0(\frac{sin\alpha_1}{\alpha_1} - \frac{sin\alpha_2}{\alpha_2}) \tag{4}$$

Obviously, at the beginning of the first increment initial rotation angle equals to zero (i.e. $\alpha_1 = 0$) which gives:

$$\Delta l = \frac{1}{2}L_0(1 - \frac{sin\alpha_2}{\alpha_2}) \tag{5}$$

3) After incremental rotation and displacement take place, the potential energy of the rest of the system (excluding the fixed blue boundary atoms) is minimized using conjugate gradient method such that the maximum force acting on the unconstrained atoms (colored in cyan) becomes less than 10^{-13} eV/Å. Then, the plots of strain energy (U), which is recorded at the end of each increment, and applied moment (M), which is calculated by the following differentiation operation, are obtained for each CNT.

$$M = \frac{dU}{d\alpha} \tag{6}$$

where U is the potential energy and α is the bending (rotation) angle (α is twice the bending angle imposed on each side of the tube). Since the changes in the energy plot can be mistaken for numerical noise, and turning points are better captured by monitoring the moment, the corresponding curve for a SWCNT with a chirality of $(m, n) = (6, 6)$, and aspect ratio of $L_0/d = 5$ is presented in Fig. 2, as an example.

[Fig. 2 should be here.]

According to the buckling mode shapes presented alongside with the variation of bending moment in Fig. 2, following observations can be made. The moment curve seems to be linear up to around 0.3 rad beyond which the slope decreases until 0.564 rad, where a slight drop, related to the occurrence of the first kink, appears. The point at which the first kink developes is referred as critical curvature (C_c). The kink deepens as the bending increases up to 1.086 rad, where an abrupt drop is observed (between 1.086 and in 1.098 rad), which denotes the transition from a single kink to a double one. Finally, the third drop happens between 1.662 and 1.674 rad as a result of the third kink.

Besides, analyzing the coordinates of the atoms reveals that the axial deformation caused by pure bending induces no coupled twist for armchair and zigzag CNTs. However, it is expected that in the case of a chiral CNT, the anisotropy in the structure brings about a coupling between axial and shear deformation, as reported in [112].

2.2 *Bending Rigidity and Critical Curvature*

Although in Section 2.1, a discussion about the variation of bending moment is provided considering a wide range of rotation angles, the focus of the present paper is going to be on the linear region which corresponds to the quadratic part of the potential energy. Accordingly, the bending stiffness (K_b) can be obtained by fitting a parabolic curve to the potential energy for the linear region:

$$K_b = \frac{d^2U}{d\alpha^2} \tag{7}$$

Since, for linear region, the bending stiffness can also be represented in terms of bending moment and bending angle (i.e. $K_b = M/\alpha$) whereas arc length (herein denotes the length of deformed CNT axis) is calculated by multiplication of the rotation angle and radius of curvature (i.e. $L_0 = \rho\alpha$), bending rigidity (K_bL_0), is derived as follows:

$$K_bL_0 = M\rho \tag{8}$$

Corresponding results (i.e. bending rigidity, critical curvature) of MD simulations are listed in Table 1 alongside with other physical features of CNTs.

[Table 1 should be here.]

Effect of Temperature and Aspect Ratio on MD results

It should be noted that decreasing the environmental temperature in MD simulations is a widely exploited approach (see Appendix 1) that mitigates the noise (scattered data) in the potential energy. Moreover, in the present study, the effect of temperature on bending rigidity and critical curvature is investigated through additional numerical experiments performed for (6,6) and (12,12) CNTs with 300 K (see Table 1): the results reveal a minor dependency of critical curvature, which is compatible with Iijima et al. [102] observation, while resulting bending rigidities turn out to be almost identical.

The independence of bending rigidity on the aspect ratio is also verified through additional simulations for slender CNTs (i.e. $L_0/d = 10, 12, 20$), where the change is less than 2%. Besides, according to Table 1, increasing the aspect ratio results in a rise in critical curvature of armchair CNTs with chirality of (5,5) and (6,6) in agreement with the findings of Cao and Chen [103]. This increase in the critical curvature can be attributed to the change in the first snap buckling configuration; As an example for SWCNT (6,6) with the aspect ratio of 5, the first buckled shape possesses only one kink, whereas, when the aspect ratio changes from 5 to 10, two kinks appear in the first buckling configuration. More discussion on the dependance of critical curvature to the aspect ratio can be found in [103].

Verification of MD results

For validation of the results of molecular dynamics simulations, a comparison to the current literature is made both on bending rigidities and critical curvatures. First of all, bending rigidities in the present work is compared with those reported by Srivastava et al. [113] and Papanikos et al. [114]. (Please note that the values for [113] are extracted from the reported plots, and those for [114] are obtained using the proposed relations for armchair and zigzag nanotubes.) As shown in Fig. 3, the findings fall within the literature data range where for zigzag CNTs, bending rigidities turn out to be slightly higher than the ones obtained for armchair CNTs, as in accordance with [113] and [114].

[Fig. 3 should be here.]

As second step of validation, critical curvature values, the variation of which illustrated in Fig. 4, are compared with those reported in the literature by Iijima et al. [102], Cao and Chen [103] and Yakobson et al. [115]. The distinct linear trend is in agreement with the findings in [102] and [115], although the curves have slopes lower than in [102] and [115] and higher than in [103]. By using the proposed relation in [102], the critical curvature of 0.162 rad/nm is attained for armchair CNTs with a chirality of (6,6). This value turns out to be close to the one obtained herein for an aspect ratio of $L_0/d = 10$ which is 0.17 rad/nm. In addition, it is observed in Fig. 4 that the overall level for critical curvature of zigzag CNTs is higher than those of armchair CNTs, especially in lower diameters. This is consistent with the predicted relation of Iijima et al. [102] in which at the same diameter, the critical curvature related to zigzag CNT is greater than the armchair counterpart with the difference more sensible in smaller diameters.

[Fig. 4 should be here.]

Exhibition of non-local and size dependent behaviour in CNT
At this point, it is checked whether CNTs exhibit non-local behavior, which calls for the use of non-classical theories for continuum modeling. For this purpose, as inspired by the studies [116], [117] and [107], a new measure, namely bending rigidity ratio, Ω, is defined to compare the results obtained from MD simulations with the Cauchy counterparts.

$$\Omega = \frac{K_b L_0}{EI} \tag{9}$$

where in the classical Cauchy formulation for pure bending of a beam, following relation holds alongside with Eq. (8):

$$M\rho = EI \tag{10}$$

with E and I being the Young's modulus and the second moment of inertia of the cross-section of the beam, respectively. Naturally, for a beam obeying Cauchy continuum, the corresponding ratio in Eq. (9) is equal to 1, while any deviation from the unity indicates non-local behavior. To adopt this relation to CNTs, the bending rigidities ($K_b L_0$), extracted from the MD simulations, are divided by the moment of inertia considering a typical thickness of 1 Å, while the results (i.e. $\Omega E = K_b L_0 / I$) are illustrated in Fig. 5 for various diameters. As most of the experiments and atomistic simulations suggest that Young's modulus (E) is insensitive to the nanotube's diameter in tensile tests [118–121], the decreasing trend of the curve with increasing diameter or vice versa indicates the presence of size-effect. This observation is consistent with an experiment conducted by Poncharal et al. [106] using electrically-induced deflections and also in accordance with the characteristic of a micropolar material in which the tubes with smaller diameters exhibit more stiffness than those with larger diameters in both bending and torsion tests [107, 116, 117, 122, 123]. As in this case, it is clear that, as the mean diameter of CNT decreases external and internal lengths become comparable resulting in a more pronounced non-locality.

[Fig. 5 should be here.]

3 Implicitly Non-local Continuum Models

This section presents the solutions to pure bending of a three-dimensional hollow cylindrical beam made of homogeneous, isotropic and linear, elastic material, in the framework of micropolar [57, 58], constrained micropolar [107] and modified couple stress [78] theories, all of which can be classified as 'implicitly' non-local models [59].

First, a solution for constrained micropolar model [107] with a displacement field equals to that of classical elastic one, and microrotations enforced to follow macro (local rigid) rotations is developed. Then, the result is improved by considering the exact displacement field obtained by Iesan [124] and presented by Reddy and Venkatasubramanian [122]. Finally, the bending problem is investigated using modified couple stress theory in which, in addition to the equality of micro and macrorotations, curvature and couple stress tensors are assumed to have a symmetric character [78].

3.1 *Constrained micropolar theory*

Consider a beam having a length of L, with a symmetrical cross-sectional area A, where z-axis, passing through the centroid of the cross-section, refers to the beam's axis, and x denoting the symmetry axis of the cross-section. The origin of cartesian coordinate system is located at the left end of the beam while a couple equal to $-M\mathbf{e}_y$ and $M\mathbf{e}_y$ is exerted on the ends with $\mathbf{e}_y$ being the unit vector in the y direction (see Fig. 6).

[Fig. 6 should be here.]

The strain field, ε_{ij} $(i, j = x, y, z)$, for a classical elastic beam subjected to bending is proved to be [125];

$$\begin{aligned} \varepsilon_{zz} &= x/\rho \\ \varepsilon_{xx} &= -\nu\varepsilon_{zz} = -\nu x/\rho \\ \varepsilon_{yy} &= -\nu\varepsilon_{zz} = -\nu x/\rho \\ \varepsilon_{xy} &= \varepsilon_{yx} = \varepsilon_{xz} = \varepsilon_{zx} = \varepsilon_{yz} = \varepsilon_{zy} = 0 \end{aligned} \tag{11}$$

where ρ is the radius of curvature, ν is the Poisson's ratio, and x is measured from the central z-axis. Similarly, the components of the curvature, χ_{ij} $(i, j = x, y, z)$, can be found as [125]:

$$\begin{aligned} \chi_{zy} &= -1/\rho \\ \chi_{yz} &= -\nu/\rho \end{aligned} \tag{12}$$

Now with considering the kinematic relations for a micropolar body;

$$\varepsilon_{ij} = u_{j,i} + e_{jik}\phi_k, \quad \chi_{ij} = \phi_{j,i} \quad (i, j, k = x, y, z) \tag{13}$$

where u_i, ϕ_i denote the displacement and microrotation components respectively, and e_{ijk} is the third order permutation tensor, following displacement and microrotation fields can be obtained by substituting the above-given strain and curvature components to the equation, and performing necessary integration operations:

$$\begin{aligned} u_x &= -(1/2\rho)[z^2 + \nu(x^2 - y^2)] \\ u_y &= -\nu xy/\rho \\ u_z &= xz/\rho \\ \phi_x &= 0 \\ \phi_y &= -z/\rho \\ \phi_z &= -\nu y/\rho \end{aligned} \tag{14}$$

Using strain and curvature fields of classical elastic problem inherently results in a displacement field equal to that of the classical one and microrotation field equal to macrorotation, θ_i, (i.e. $\phi_i = \theta_i = \frac{1}{2}e_{ijk}u_{k,j}$). It should be noted that, the afore-mentioned assumptions on displacement and microrotation fields are first proposed by Lake [107] for deriving the bending rigidity ratio of a beam with rectangular cross-section and it is revisited here for the general case of any micropolar beam with symmetrical cross-section.

The constitutive relation for a linear elastic micropolar continuum is represented as

$$\sigma_{ij} = \lambda\varepsilon_{kk}\delta_{ij} + \mu\varepsilon_{ji} + (\mu+\kappa)\varepsilon_{ij}, \quad \mu_{ij} = \alpha\chi_{kk}\delta_{ij} + \beta\chi_{ji} + \gamma\chi_{ij} \quad (i,j,k = x,y,z) \tag{15}$$

which contains six elastic material constants; the two Lamé λ, and μ constants and four additional material constants, α, β, γ and κ emerging from micropolar theory. The following so-called engineering constants are also derived based on the aforementioned six parameters for providing better physical insight [107]:

$$\begin{aligned}
G =& \mu + \kappa/2 \quad \text{: shear modulus} \\
N =& \sqrt{\kappa/(2(\mu+\kappa))} \quad \text{: coupling number} \\
l_t =& \sqrt{(\beta+\gamma)/(2\mu+\kappa)} \quad \text{: characteristic length for torsion} \\
\psi =& (\beta+\gamma)/(\alpha+\beta+\gamma) \quad \text{: polar ratio} \\
E =& (2\mu+\kappa)(3\lambda+2\mu+\kappa)/(2\lambda+2\mu+\kappa) \quad \text{: Young's modulus} \\
\nu =& \lambda/(2\lambda+2\mu+\kappa) \quad \text{: Poisson's ratio} \\
l_b =& \sqrt{\gamma/2(2\mu+\kappa)} \quad \text{: characteristic length for bending}
\end{aligned} \tag{16}$$

With substituting the strain and curvature fields, given in Eqs (11) and (12), into the Eq. (15), the only non-vanishing stress and couple stress components become:

$$\begin{aligned}
\sigma_{zz} &= Ex/\rho \\
\mu_{zy} &= -\frac{\beta\nu+\gamma}{\rho} \\
\mu_{yz} &= -\frac{\beta+\gamma\nu}{\rho}
\end{aligned} \tag{17}$$

where E refers to Young's modulus and can be represented in terms of other material constants; $E = (2\mu+\kappa)(3\lambda+2\mu+\kappa)/(2\lambda+2\mu+\kappa)$.

Requiring that the resultant moment on each plane normal to the z-axis is equal to the applied moment, following equation is obtained:

$$\int_A (-x\sigma_{zz} + \mu_{zy})\, dA = -M \tag{18}$$

Note that the moment around the x-axis, related to $y\sigma_{zz}dA$, vanishes since the application of couples in the plane of symmetry results in a symmetric distribution of normal stresses about this axis.

With further substituting the expressions for σ_{zz} and μ_{zy}, given in Eq. (17), into the Eq. (18), the below-given relation, which denotes $M\rho$; the bending rigidity of the micropolar beam, is obtained:

$$EI + (\beta\nu+\gamma)A = M\rho \tag{19}$$

where, I is the second moment of inertia about the y-axis.

Analogous to Eq. (9) in Section 2.2 and inspired by the studies [116], [117] and [107], the non-dimensional micropolar bending rigidity ratio, Ω_{m}, is defined as the ratio

of bending rigidity of a micropolar beam to that of its classical counterpart. Since $M\rho$ is the observed bending rigidity of the micropolar beam, while EI is the corresponding classical value, Ω_{m} can be obtained by dividing both sides of Eq. (19) by EI as follows:

$$\Omega_{\mathrm{m}} = \frac{M\rho}{EI} = 1 + \frac{(\beta\nu + \gamma)A}{EI} \tag{20}$$

Although the lateral surface of the beam should be free of not only tractions, but also couple tractions, substituting the stress and couple stress components into the below-given relations,

$$t_i = \sigma_{ji} n_j, \qquad \mu_i = \mu_{ji} n_j \qquad (i, j = x, y, z) \tag{21}$$

yields non-zero couple traction due to μ_{yz}. This couple stress component is the only component that prohibits the present solution to be exact. So, the solution is exact only when $\frac{\beta}{\gamma} = -\nu$. It should be noted that although Eq. (20) may not be exact, a similar approach with the same constraint is proposed by Lake [107] for the bending rigidity of a micropolar beam with rectangular cross section which is further adopted in various studies [126–129]. An even more simplified version of this formulation neglecting χ_{yz} is also used by some other researchers [130–132].

Finally, by using the relations of $l_b^2 = \gamma(1+\nu)/2E$ and $-\nu = \frac{\beta}{\gamma}$, Eq. (20) is rewritten as:

$$\Omega_{\mathrm{cm}} = 1 + 2\,(1-\nu)\, l_b^2\, \frac{A}{I} \tag{22}$$

which can be further adopted as follows considering hollow circular cross-section with R_o and R_i being the outer and inner radii:

$$\Omega_{cm} = 1 + 8\,(1-\nu)\, \frac{l_b^2}{R_o^2 + R_i^2} \tag{23}$$

3.2 *Micropolar theory*

The solution procedure in this section is based on a study by Reddy and Venkatasubramanian [122] for determining the bending rigidity of a micropolar hollow circular cylinder. Here, the problem is restated from a more comprehensible perspective, and more details are provided. In this case, to obtain the solution for the bending rigidity of a micropolar hollow cylinder, a general displacement field is considered as follows:

$$\begin{aligned}
u_x &= -(1/2\rho)[z^2 + \nu(x^2 - y^2)] + (1/\rho)u^p(x,y) \\
u_y &= -\frac{\nu xy}{\rho} + (1/\rho)v^p(x,y) \\
u_z &= xz/\rho \\
\phi_x &= 0 \\
\phi_y &= -z/\rho \\
\phi_z &= -\frac{\nu y}{\rho} + (1/\rho)\phi^p(x,y)
\end{aligned} \tag{24}$$

which is consistent with the exact solution proposed by Iesan [124]. As a matter of fact, the additional terms of $u^p(x,y)$, $v^p(x,y)$ and $\phi^p(x,y)$ are added to the displacement field in Eq. (14) to adjust the boundary condition related to free surface couple traction which couldn't be satisfied in Section 3.1. Here, the subscript p refers to the plane problem.

As all the equations are in a linear elastic framework, the solution to the bending of a micropolar hollow cylinder can be obtained by superposing the solution in the previous section with the solution related to a plane problem corresponding to $u^p(x,y)$, $v^p(x,y)$ and $\phi^p(x,y)$, which can be represented in polar coordinates as:

$$\begin{aligned} u_z^p &= \phi_r^p = \phi_\theta^p = 0 \\ \phi_z^p &= \phi^p(r,\theta) \\ u_r^p &= u^p(r,\theta) \\ u_\theta^p &= v^p(r,\theta) \end{aligned} \tag{25}$$

while subjected to following boundary conditions:

$$\begin{aligned} &\mu_{rz}^p = (\beta+\gamma\nu)\sin(\theta)\ , \quad r = R_i \text{ and } r = R_o \\ &\sigma_{r\theta}^p = 0, \quad r = R_i \text{ and } r = R_o \end{aligned} \tag{26}$$

Note that substituting the plane stress displacement field in Eq. (25) into the constitutive relation (Eq. (15)), already gives $\mu_{rr}^p = \mu_{r\theta}^p = 0$, and thus it has not appeared in Eq. (26).

By substituting Eq. (13) into Eq. (15) and a further substitution into the following balance equation [57],

$$\sigma_{ji,j} = 0, \qquad \mu_{jk,j} - e_{ijk}\sigma_{ji} = 0 \tag{27}$$

the governing equations of a micropolar continuum can be written as follows in terms of displacement field:

$$\begin{aligned} &(\lambda+\mu)u_{i,ik}^p + (\mu+\kappa)u_{k,ii}^p + \kappa e_{kij}\phi_{j,i}^p = 0 \\ &(\alpha+\beta)\phi_{i,ik}^p + \gamma\phi_{k,ii}^p + \kappa e_{kij}u_{j,i}^p - 2\kappa\phi_k^p = 0 \quad (i,j,k = r,\theta,z) \end{aligned} \tag{28}$$

Chui and Lee, derived the general solution to this plane problem with the general boundary condition expanded in the Fourier series [133]:

$$\begin{aligned} u_r^p &= u^p(r,\theta) = \sum_{n=-\infty}^{\infty} U_n(r)e^{in\theta} \\ u_\theta^p &= v^p(r,\theta) = \sum_{n=-\infty}^{\infty} iV_n(r)e^{in\theta} \qquad n = 0,\pm1\ ,\pm2,\ \ldots \\ \phi_z^p &= \phi^p(r,\theta) = \sum_{n=-\infty}^{\infty} i\Phi_n(r)e^{in\theta} \end{aligned} \tag{29}$$

The relations for the Fourier coefficients for each n are proposed in [133]. Here, considering the boundary conditions in Eq. (26), the coefficients related to $n = 1$ is picked out as follows;

$$
\begin{aligned}
\mathrm{U}(r) =& A_1 - \frac{k}{2(2\mu+\kappa)(1+c)}A_2 + \left[1 + \frac{\kappa}{(2\mu+\kappa)(1+c)}\right]A_2 \ln r \; + \left[1 + \frac{\kappa}{(2\mu+\kappa)(1-3c)}\right]A_3 r^2 \\
&+ A_4 r^{-2} + \frac{k}{2(\mu+\kappa)\delta}\{A_5[K_2(\delta r) - K_0(\delta r)] - A_6[I_2(\delta r) - I_0(\delta r)]\} \\
\mathrm{V}(r) =& A_1 + \frac{A_2}{(1+c)}\left[1 - c + \frac{k}{2(2\mu+\kappa)}\right] + \left[1 + \frac{\kappa}{(2\mu+\kappa)(1+c)}\right]A_2 \ln r \\
&+ \frac{A_3}{1-3c}\left[3 - c + \frac{3\kappa}{2\mu+\kappa}\right]r^2 - A_4 r^{-2} + \frac{k}{2(\mu+\kappa)\delta}\{-A_5[K_2(\delta r) + K_0(\delta r)] \\
&+ A_6[I_2(\delta r) + I_0(\delta r)]\} \\
\Phi(r) =& A_5 K_1(\delta r) + A_6 I_1(\delta r) + \frac{\mu+\kappa}{2\mu+\kappa}\left[\frac{2}{1+c}A_2 r^{-1} + \frac{8}{1-3c}A_3 r\right]
\end{aligned}
\tag{30}
$$

where I_n and K_n are the modified Bessel functions of the first and second kind of order n.

The expressions for Fourier coefficients of stress components are also presented in [133]. The coefficients A_1 to A_6 , can be obtained by using the boundary conditions in Eq. (26), which yields to the following system of linear equations to achieve the exact solution of the problem;

$$
\begin{bmatrix}
2I_1'(\delta R_i) & 2K_1'(\delta R_i) & 8N^2 & 0 \\
2I_1'(\delta R_o) & 2K_1'(\delta R_o) & 8N^2 & 0 \\
-I_2(\delta R_i) & K_2(\delta R_i) & \frac{(\delta R_i)^2}{2(1-\nu)} & \frac{1}{(\delta R_i)^2} \\
-I_2(\delta R_o) & K_2(\delta R_o) & \frac{(\delta R_0)^2}{2(1-\nu)} & \frac{1}{(\delta R_o)^2}
\end{bmatrix}
\begin{bmatrix}
-\frac{\delta N^2 A_6}{2} \\
-\frac{\delta N^2 A_5}{2} \\
\frac{-A_3}{2(1-N^2)(1-3c)} \\
\frac{-N^2(2\mu+\kappa)\delta^2 A_4}{\gamma}
\end{bmatrix}
= N^2(\nu + \beta/\gamma)
\begin{bmatrix}
1 \\ 1 \\ 0 \\ 0
\end{bmatrix}
\tag{31}
$$

where $\delta^2 = \kappa(2\mu+\kappa)/\gamma(\mu+\kappa)$ and $c = (\mu+\kappa)/(\lambda+2\mu+\kappa)$. Finally, the total σ_{zz} and μ_{zy} of the main problem can be written as;

$$
\begin{aligned}
\sigma_{zz} =& \frac{Ex}{\rho} + \frac{\sigma_{zz}^p}{\rho} \\
\mu_{zy} =& -\frac{\beta\nu + \gamma}{\rho} + \frac{\mu_{z\theta}^p cos(\theta) + \mu_{zr}^p sin(\theta)}{\rho}
\end{aligned}
\tag{32}
$$

By substituting σ_{zz} and μ_{zy} given in Eq. (32) into the resultant moment equation (Eq. (18)), and by dividing the obtained $M\rho$ with the second moment of inertia about y-axis, (i.e. $I = \pi E({R_o}^4 - {R_i}^4)/4$), the final relation for the bending rigidity ratio of a micropolar hollow cylinder is derived:

$$
\Omega_{\mathrm{m}} = 1 + \frac{8N^2}{1+\nu}\left[\frac{1 - (\beta/\gamma)^2}{(\delta R_i)^2 + (\delta R_o)^2} + \frac{(\nu + \beta/\gamma)^2}{8N^2(1-\nu) + \xi(\delta R_i, \delta R_o)}\right]
\tag{33}
$$

where

$$\begin{aligned}\xi\left(\delta R_i, \delta R_o\right) = & \left[\left(\delta R_o\right)^4 - \left(\delta R_i\right)^4\right]\left[I_1'\left(\delta R_i\right) K_1'\left(\delta R_o\right) - K_1'\left(\delta R_i\right) I_1'\left(\delta R_o\right)\right] \\ & \times \left[\left\{I_1'\left(\delta R_o\right) - I_1'\left(\delta R_i\right)\right\}\left\{\left(\delta R_o\right)^2 K_2\left(\delta R_o\right) - \left(\delta R_i\right)^2 K_2\left(\delta R_i\right)\right\}\right. \\ & \left. + \left\{K_1'\left(\delta R_o\right) - K_1'\left(\delta R_i\right)\right\}\left\{\left(\delta R_o\right)^2 I_2\left(\delta R_o\right) - \left(\delta R_i\right)^2 I_2\left(\delta R_i\right)\right\}\right]^{-1}\end{aligned} \tag{34}$$

and

$$\begin{aligned}K_1'\left(\delta R_o\right) &= -\frac{1}{2}\left(K_2\left(\delta R_o\right) + K_0\left(\delta R_o\right)\right) \\ I_1'\left(\delta R_o\right) &= \frac{1}{2}\left(I_2\left(\delta R_o\right) + I_0\left(\delta R_o\right)\right)\end{aligned} \tag{35}$$

3.3 *Modified couple stress theory*

In this section, the formulation for pure bending of a hollow cylinder in the modified couple stress theory framework is derived. In the couple stress theory, the microrotations are constrained to follow the local rigid rotation which results in the symmetry of strains and stresses. However, in modified couple stress theory, proposed by Yang et al [78], in addition to this constraint, the curvatures and couple stresses are also considered to be symmetric. The displacement and microrotation fields in this section is assumed to be the same as Eq. (14) in Section 3.1, where the displacement field is equal to that of the classical case and the microrotation equals to the macrorotation. Then, the kinematic relations in the modified couple stress theory will be [78]:

$$\begin{aligned}\varepsilon_{ij} &= \frac{1}{2}\left(u_{i,j} + u_{j,i}\right) \\ \chi_{ij} &= \frac{1}{2}\left(\phi_{i,j} + \phi_{j,i}\right)\end{aligned} \tag{36}$$

while the constitutive equations are read [78]:

$$\begin{aligned}\sigma_{ij} &= \lambda\varepsilon_{kk}\delta_{ij} + 2\mu\varepsilon_{ij} \\ m_{ij} &= 2l^2\mu\chi_{ij}\end{aligned} \tag{37}$$

where l becomes the only internal length scale parameter and m_{ij} is the deviatoric part of the couple stress tensor. Since in the present problem μ_{ii}= 0, the equality of μ_{ij}=m_{ij} holds.

The stress and couple stress components of σ_{zz} and μ_{zy} are determined by substituting the displacement field (Eq. (14)) into Eq. (36), followed by a further substitution into Eq. (37):

$$\begin{aligned}\sigma_{zz} &= \frac{Ex}{\rho} \\ \mu_{zy} = m_{zy} &= -2l^2\mu\frac{1+\nu}{2\rho} = -\frac{El^2}{2\rho}\end{aligned} \tag{38}$$

As the equilibrium relation in Eq. (18) also holds here, substituting Eq. (38) into Eq. (18) gives:

$$EI + \frac{El^2}{2}A = M\rho \tag{39}$$

By dividing Eq. (39) with the classical bending rigidity, gives the bending rigidity ratio for the case of modified couple stress theory (Ω_{cs}):

$$\Omega_{cs} = \frac{M\rho}{EI} = 1 + \frac{l^2}{2}\frac{A}{I} \tag{40}$$

which takes the following form considering a hollow circular cross-section:

$$\Omega_{cs} = \frac{M\rho}{EI} = 1 + \frac{2l^2}{R_o^2 + R_i^2} \tag{41}$$

Finally, it should also be noted that in the case of Cauchy theory, no size effect is observed and the bending rigidity ratio, Ω_{Cauchy}, equals to unity.

For more clarity, a summary of the kinematic and constitutive equations for the three continuum theories mentioned in this section are provided in Table 2.

[Table 2 should be here.]

4 Determination of Material Parameters

In this section, CNTs are considered as equivalent three-dimensional hollow cylindrical beams made of homogeneous, isotropic, linear and elastic material described by non-classical micropolar, constrained micropolar, modified couple stress and classical Cauchy theories. To determine the corresponding constitutive parameters, a non-linear optimization approach, aiming to minimise the difference between bending rigidities obtained from MD simulations and continuum models, is employed.

4.1 *Optimization Problem*

Optimization process is performed by utilising *lsqnonlin* command, a non-linear least-square solver with optional lower and upper bounds that use the trust-region-reflective algorithm, in MATLAB software [134] to search for following properties:

$$\min\{F_{obj}(E, \nu, l_b, N, \frac{\beta}{\gamma}, h)\} \tag{42}$$

with F_{obj} being the non-linear objective function that is defined as the Euclidean norm of the difference between the bending rigidities, attained from MD simulations, $K_b L_0$, (Section 2.2), and continuum relations, ΩEI, (Section 3):

$$F_{obj} = \left| \frac{(K_b L_0)_{\text{MD}} - (\Omega EI)_{\text{continuum}}}{(K_b L_0)_{\text{MD}}} \right| \tag{43}$$

Considering the principle of non-negative energy, and Vodenitcharova and Zhang criterion [135], the below given inequality constraints are defined.

$$0 \leq E,\ \ -1 < \nu \leq 0.5\ ,\ \ 0 \leq l_b,\ \ 0 \leq N \leq 1,\ \ -1 \leq \frac{\beta}{\gamma} \leq 1,\ \ 0 \leq h \leq 1.42 \tag{44}$$

Once the unknowns in Eq. (42) are determined, the other constitutive parameters can be derived by exploiting the relations in Eq. (16), as follows:

$$\begin{aligned} &G = \frac{E}{2\,(1+\nu)},\ \ \gamma = 4Gl_b^2\ ,\ \ \beta = \frac{\beta}{\gamma}\gamma,\ \ l_t = \sqrt{\frac{\beta+\gamma}{2G}} \\ &\lambda = \frac{2G\nu}{1-2\nu},\ \ k = \frac{2GN^2}{1-N^2},\ \ \ \mu = G - \frac{k}{2} \end{aligned} \tag{45}$$

At this point, it should be mentioned that, in case of the constrained micropolar formulation, the unknown parameters reduce to $E,\ \nu,\ l_b$ and h, whereas for modified couple stress theory there will be three; E , l and h, and for Cauchy theory there will be only in-plane stiffness; Eh.

Note that an optimization problem is considered non-linear if the objective function and/or the constraints are non-linear, and non convex if the constraints define a non convex problem. The existence and uniqueness of the solution can be guaranteed by Kuhn-Tucker conditions [136]. In the present problem, F_{obj} is a non-linear function with the inequality constraints (i.e. Eq. (44)), that define a non convex domain. Although, in this case the existence and uniqueness of the solution is not guaranteed, with a proper selection of initial guesses a feasible and local minimum solution has been found for the problem.

[Table 3 should be here.]

4.2 *Results and Discussion*

By adopting the above-mentioned optimization procedure and exploiting the relations given in Eq. (45), the unknown parameters for armchair and zigzag CNTs as equivalent three-dimensional hollow cylindrical beams are determined, and presented in Table 3, for micropolar, constrained micropolar, modified couple stress and Cauchy theories. Here, for comparison, a fixed thickness of 1.01 Å (the one obtained in micropolar case) is imposed on the problems adopting modified couple stress and constrained micropolar theories, as this additional constraint does not yield any significant difference in the norm of their objective functions, whereas a freedom in the choice of the thickness exists for the Cauchy model.By using the corresponding identified parameters, the variation of bending modulus predicted by continuum theories are plotted alongside with those already obtained from MD simulations (see Fig. 7). Besides, as the results of the atomistic simulation are not significantly affected by the temperature in the range of 0 to 300 K, the obtained material parameters are applicable for this temperature range.

As mentioned in the previous paper of some of the Authors [100], the solution of the non-linear optimization problem naturally depends on the initial guesses, such that different initial guesses for Young's modulus lead to different optimised values of

E and h, while the product of Eh is almost constant (about 0.289-0.296 TPa.nm), as consistent with the physical nature of CNTs in tensile loading.

Prediction of size effect in bending modulus

As inferred from Table 3, the use of constrained micropolar, modified couple stress and Cauchy theories increases the norm of the objective function. This variation is especially pronounced for Cauchy, which turns out 26 (for armchair) and 44 (for zigzag) times greater than the one obtained for micropolar theory; hence, points out the necessity of including material parameters accounting for scale effects. Moreover, it is also evident from Fig. 7, that the evaluation of bending modulus is best captured by micropolar theory, which inherently accounts for the relative rotations related to the skew-symmetric part of the strain tensor, whereas the almost identical prediction by the modified couple stress theory and constrained micropolar theory can be interpreted as acceptable and valuable considering their relatively simple formulations. Meanwhile, the incapability of the Cauchy theory in capturing size-effects is once more revealed.

Bending characteristic length

The fact that the present method leads to unique internal characteristic length (l_b), independent of the diameter and chirality of CNTs, with a consistent physical interpretation, which turns out to be directly related to the carbon-carbon bond length (i.e. $\approx$ 1.4 Å), is a very distinct feature, as in the majority of the literature (e.g. [94], [99], [82], [137], [138], [99], [139]), either a predefined fixed value is used for non-locality related parameters or it is found to vary with aspect ratio, diameter, and other features. On the other hand, the values that are determined using modified couple stress theory and constrained micropolar theory are 1.08 Å and 0.66 Å for armchair and 1.18 Å and 0.71 Å for zigzag CNTs, respectively. The predictions seem to be acceptable considering their simplicity.

Young's modulus and Poisson's ratio

For comparison, the reported Young's modulus and Poisson's ratio values, that are obtained by performing atomistic simulations, analytical calculations and/or experiments, are summarised in Table 4. Since assuming different values for CNTs' thickness (ranging from 0.617 Å to 6.9 Å [37]) resulting in a large discrepancy in Young's modulus, it is common to compare in-plane stiffness (Eh), for which a narrower range (from 0.234 TPa.nm to 0.612 TPa.nm) exists. The presented optimised value of in-plane stiffness that is determined for micropolar theory differs less than 1% from the ones given by Hu et al. [140], in which tensile characteristics of armchair CNTs are investigated through MD simulations. Moreover, as one can see from Table 3, the value of in-plane stiffness turns out to be almost independent of the adopted continuum theory; i.e. the largest difference, which is about 8%, is between non-classical micropolar and classical Cauchy theories. Regarding Poisson's ratio, there is a considerable inconsistency in literature varying from 0.14 to 0.41 (see Table 4) while the obtained value of $\nu = 0.253$ falls well within this data and is near to those obtained by Hu et al. [140].

[Fig. 7 should be here.]

Comparison with the torsional loading results

In order to check the independence of the identified parameters from the loading protocol, the common material properties in the Authors' previous work [100] based on torsion test data is compared with the ones presented herein. Although the results are not reproduced precisely, acceptable values are attained, especially for armchair nan-

otubes; i.e. considering micropolar theory, the torsional characteristic length, l_t, that is calculated by using the relation given in Eq. (45), is 2.77 Å, and differs about 17% from the one in Izadi et al. [100]. Also, the discrepancy between the shear modulus in the two loading protocols is less than 3% with about 18% difference for the coupling numbers. Since the bending test lead to smaller norms of objective function, it can be concluded that, the results (i.e. optimised parameters) have been improved compared to torsion test. It is because in bending simulation, the energy minimisation is used at each increment, which considerably reduces the fluctuations of the results, and also a method is proposed to relax the induced spurious axial strain during loading.

The Effect of Chirality

The results (see Table 3 and Fig.7) point out the almost negligible effect of the orientation of the hexagonal carbon rings on the elastic properties with a maximum differences of 6% for micropolar constant, κ, whereas Young's modulus varies less than 1% and is in agreement with the literature [114, 120, 141, 142]. Even though a more pronounced discrepancy is obtained for constrained micropolar (15%, 16%, and 8% for γ, β and l_b, respectively) and modified couple stress (9% for l_b) theories, the predictions of micropolar theory, endowed with relative rotations, can be considered as more precise and more reliable to be deduced from. Due to the small difference between obtained material parameters for two distinct classes of chirality; i.e., zigzag (n=0) and armchair (m=n), the results are expected to remain within this range considering CNTs with arbitrary chirality. In fact, through further numerical experiments, an empirical formulation between chiral indices (m,n) and constitutive properties can be derived yet not investigated in this study. Besides, the procedure presented herein can be easily applied for multi-walled CNTs to obtain equivalent material parameters. Alternatively, the values attained for each SWCNT wall in the present work can be incorporated in a continuum method to model a multi-walled CNT considering an equivalent stiffness for the van der Waals layers.

[Table 4 should be here.]

5 Conclusion

A comprehensive examination of the mechanical response of carbon nanotubes (CNTs) is still in progress, while frequently employed discrete modeling techniques are suffering from high computational cost, and performing actual experiments tends to be physically challenging. In this regard, balancing accuracy with computational efficiency can be achieved by means of continuum models that are calibrated through atomistic simulations, whereas a suitable choice of the theory has the utmost significance, especially in the presence of scale effects.

In this paper, first, a systematic procedure ensuring pure bending using molecular dynamics (MD) simulations is employed to investigate flexural behavior of armchair and zigzag single-walled CNTs (SWCNTs) with moderately small aspect ratio (i.e. $L_0/d \approx 5$). This is achieved by introducing a method that keeps the length of the deformed CNT axis unaltered, and eliminates the errors that might be developed due to misuse of boundary conditions. The results evidently demonstrate the effect of size-dependence on the bending modulus; i.e. nanotubes with smaller diameters ex-

hibit higher bending modulus in contrast to the classical case for which it is expected to remain constant; hence, indicates the necessity of adopting enhanced non-classical (non-local) theories. The observed size effect in bending modulus is attributed to the fact that mean diameter (external length) of the studied CNTs are comparable to the lattice spacing (internal length) between the individual atoms. Second, the capacity of micropolar, constrained micropolar and modified couple stress theories is investigated, while CNTs are modelled as three-dimensional hollow cylindrical beams made of homogeneous, isotropic, linear and elastic material. Through a non-linear optimization approach, that enforces equivalency between atomistic observation and continuum prediction, in terms of bending rigidity, constitutive parameter sets for each class of chirality are determined. The results reveal the great potential of micropolar theory, allowing for relative rotations, in capturing the observed size effect as the predicted bending modulus perfectly fits the corresponding MD-simulated data. Even though such an agreement is not achieved for modified couple stress and deformation-wise constrained micropolar theories, a sufficient accuracy is still provided despite their over-simplified formulations. On the other hand, the inadequacy of classical Cauchy theory in predicting the scale effects is once more proven as the memory of underlying structure, which strongly affects the overall mechanical behavior, cannot be retained.

As interesting features of the presented study, the value of the internal scale parameter, l_b, turns out to be directly correlated to the carbon-carbon bond length (≈ 1.4 Å), while the comparison of the material parameters obtained from the bending test given herein, and the torsion test given in the Authors' previous contribution [100] concludes the independence of the results from selected loading scenarios. Moreover, the identified material parameter sets are valid for all armchair and zigzag nanotubes with various lengths since bending rigidity, which is used in optimization process, proved to be independent of the aspect ratio. However, further study is required to ensure the extension of the results for CNTs with considerably large values of aspect ratio.

Table 1: Properties, critical curvatures (C_c) and bending rigidities ($K_b L_0$) of armchair and zigzag CNTs with different diameters.

	Chirality (m,n)	**Diameter (Å)**	**Temp. (K)**	**Crt. Curv. (rad/nm)**	**Length (nm)**	**Aspect Ratio**	**Bend. Rig. (nN.(nm)²)**
	(5,5)	6.78	10	0.207	3.28	4.8	41.1
	(5,5)	6.78	10	0.250	8.15	12.0	40.5
	(5,5)	6.78	10	> 0.23	13.50	19.9	40.3
	(6,6)	8.09	10	0.141	4.01	5.0	68.1
	(6,6)	8.09	10	0.170	8.14	10.1	67.5
	(6,6)	8.09	300	0.170	8.15	10.1	67.8
Armchair	(7,7)	9.42	10	0.103	4.73	5.0	105.1
	(8,8)	10.74	10	0.080	5.46	5.1	153.9
	(9,9)	12.07	10	0.064	6.18	5.1	215.4
	(10,10)	13.40	10	0.052	6.66	5.0	293.1
	(11,11)	14.73	10	0.044	7.39	5.0	386.3
	(12,12)	16.06	10	0.037	8.11	5.1	496.7
	(12,12)	16.06	10	0.044	16.11	10.0	490.8
	(12,12)	16.06	300	0.042	16.11	10.0	491.3
	(8,0)	6.33	10	0.296	3.06	4.8	34.4
	(10,0)	7.84	10	0.175	3.91	5.0	62.5
	(12,0)	9.36	10	0.120	4.75	5.1	103.4
Zigzag	(14,0)	10.89	10	0.088	5.30	4.9	159.6
	(16,0)	12.42	10	0.068	6.14	4.9	233.6
	(18,0)	13.95	10	0.054	6.84	4.9	328.2
	(20,0)	15.48	10	0.044	7.82	5.1	444.6
	(21,0)	16.25	10	0.040	8.24	5.1	511.0

Table 2: Comparison of kinematic and constitutive equations in micropolar, constrained micropolar and modified couple stress theories

	micropolar	**constrained micropolar**	**modified couple stress**
strain	$\varepsilon_{ij} = u_{j,i} + e_{jik}\phi_k$ $= \frac{1}{2}\left(u_{j,i} + u_{j,i}\right) + e_{ijk}(\theta_k - \phi_k)$	$\varepsilon_{ij} = u_{j,i} + e_{jik}\phi_k$ $\xrightarrow{\theta_k=\phi_k}$ $= \left(u_{j,i} + u_{j,i}\right)/2$	$\varepsilon_{ij} = \frac{1}{2}\left(u_{j,i} + u_{j,i}\right)$
curvature	$\chi_{ij} = \phi_{j,i}$	$\chi_{ij} = \phi_{j,i}$	$\chi_{ij} = \left(\phi_{i,j} + \phi_{j,i}\right)/2$
stress	$\sigma_{ij} = \lambda\varepsilon_{kk}\delta_{ij} + \mu\varepsilon_{ji} + (\mu+\kappa)\varepsilon_{ij}$	$\sigma_{ij} = \lambda\varepsilon_{kk}\delta_{ij} + \mu\varepsilon_{ji} + (\mu+\kappa)\varepsilon_{ij}$ $\xrightarrow{\varepsilon_{ij}=\varepsilon_{ji}}$ $\sigma_{ij} = \lambda\varepsilon_{kk}\delta_{ij} + (2\mu+\kappa)\varepsilon_{ij}$	$\sigma_{ij} = \lambda\varepsilon_{kk}\delta_{ij} + 2\mu\varepsilon_{ij}$
couple stress	$\mu_{ij} = \alpha\chi_{kk}\delta_{ij} + \beta\chi_{ji} + \gamma\chi_{ij}$	$\mu_{ij} = \alpha\chi_{kk}\delta_{ij} + \beta\chi_{ji} + \gamma\chi_{ij}$ $\xrightarrow{\chi_{kk}=0}$ $\mu_{ij} = \beta\chi_{ji} + \gamma\chi_{ij}$	$m_{ij} = 2l^2\mu\chi_{ij}$

Table 3: Identified material parameters for armchair and zigzag CNTs

		micropolar	**constrained micropolar**	**modified couple stress**	**Cauchy**
	E (GPa)	2865	2962	2962	3090
	N	0.18	-	-	-
	β/γ	0.93	-	-	-
	ν	0.25	0.33	-	-
	l_b (Å)	1.409	0.66	1.08	-
	h (Å)	1.01	1.01	1.01	1.01
	Eh (TPa.nm)	0.291	0.3	0.3	0.313
	F_{obj}	0.0026	0.0075	0.0075	0.069
armchair	G (GPa)	1144	1116	-	-
	γ (nN)	91	19	-	-
	β (nN)	85	-6	-	-
	λ (GPa)	1167	2116	-	-
	κ (GPa)	79	-	-	-
	μ (GPa)	1104	-	-	-
	$\beta+\gamma$ (nN)	175	-	-	-
	l_t (Å)	2.77	0.76	-	-
	E (GPa)	2837	2932	2932	3086
	N	0.19	-	-	-
	β/γ	0.91	-	-	-
	ν	0.25	0.3	-	-
	l_b (Å)	1.416	0.71	1.18	-
	h (Å)	1.01	1.01	1.01	1.01
	Eh (TPa.nm)	0.288	0.297	0.297	0.313
	F_{obj}	0.0022	0.0088	0.0088	0.096
zigzag	G (GPa)	1139	1127	-	-
	γ (nN)	91	22	-	-
	β (nN)	83	-7	-	-
	λ (GPa)	1102	1706	-	-
	κ (GPa)	84	-	-	-
	μ (GPa)	1097	-	-	-
	$\beta+\gamma$ (nN)	175	-	-	-
	l_t (Å)	2.768	0.83	-	-

Table 4: Comparative study on the in-plane stiffness (Eh) and Poisson's ratio (ν)

	Eh(TPa.nm)	**SWCNT**	**loading**	**method**	ν
Atomistic simulation/Analytical Methods					
Present Work	0.291	(5,5) to (12,12)	Bending	MD-AIREBO potential	0.253
Arroyo & Belytschko [143]	0.234	(10,10)	-	exponential Cauchy-Born rule	0.41
Hu et al. [140]	0.303	(5,5)	Tensile	MD-REBO potential	0.25
Hu et al. [140]	0.282	(10,10)&(15,15)	Tensile	MD-REBO potential	0.317
Vodenitcharova & Zhang [135]	0.301	-	external hydrostatic pressure	ring theory of continuum mechanics	-
Lu [121]	0.329	(5,5)-(200,200)	Tensile	Empirical force-constant model	0.28
Kudin et al. [119]	0.330-0.338	(4,4)-(7,7)-(7,0)-(12,0)	Tensile	ab-initio methods	0.14-0.18
Yakobson et al. [115]	0.363	-	Tensile	Tersoff-Brenner potential	0.19
Hernandz et al. [120]	0.416-0.430	(6,6)-(15,15)	Tensile	nonorthogonal tight binding	-
Experiment					
Demczyk et al. [144]	0.306		Bending	bending tests on individual carbon nanotubes in-situ in a TEM	-
Salvetat et al. [145]	0.306	mean Diameter 1.4 nm	Bending	with AFM	-
Treacy et al. [146]	$0.612^{+0.799}_{-0.476}$		Thermal vibration	captured with TEM	-
Krishnan et al. [147]	$0.442^{+0.204}_{-0.136}$	27 nanotubes in the diameter range 1.0–1.5 nm	Thermal vibration	captured with TEM	-
Wong [148]	$0.435^{+0.2}_{-0.2}$		Bending	Cantilever bending by AFM	-

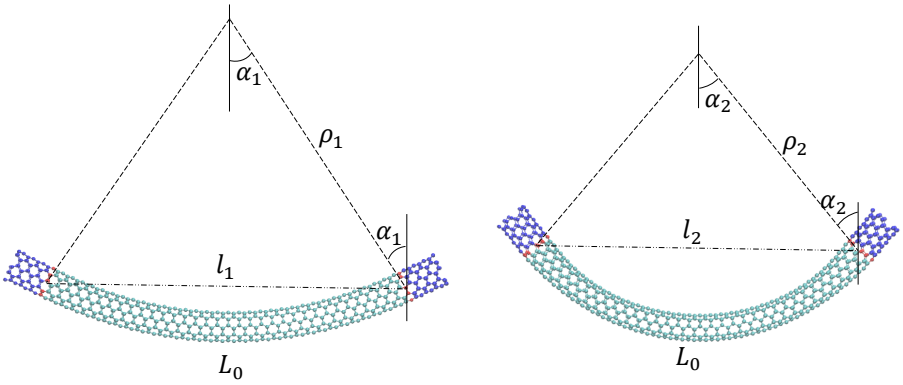

Figure 1: Schematic of the rotation angle (α), radius of curvature (ρ) and end-to-end distance (l) at the beginning and end of an increment during pure bending, illustrated for an armchair single-walled carbon nanotube with a chirality of $(m, n) = (5, 5)$ and aspect ratio of $L_0/d = 12$ (The changes are exaggerated)

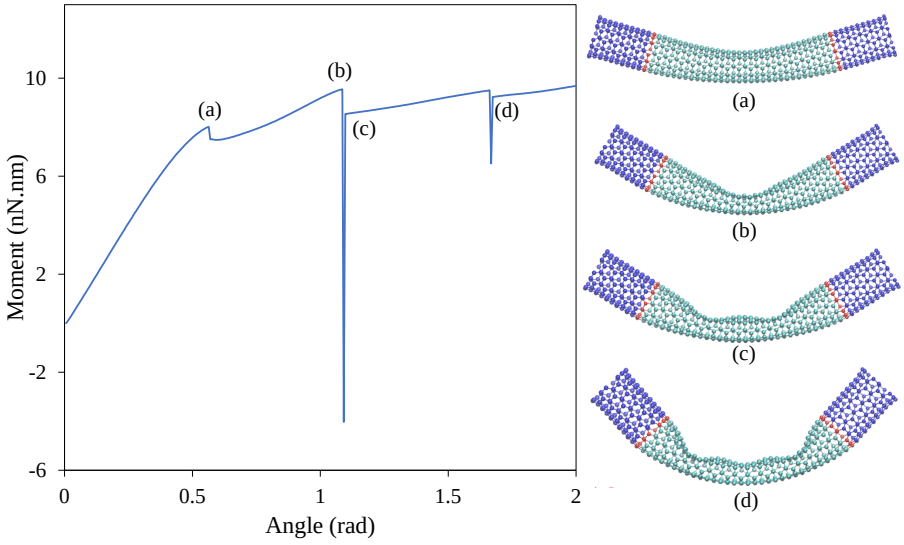

Figure 2: Plots of applied moment of single-walled carbon nanotube with a chirality of $(m, n) = (6, 6)$ and aspect ratio of $L_0/d = 5$ alongside with corresponding buckling mode shapes

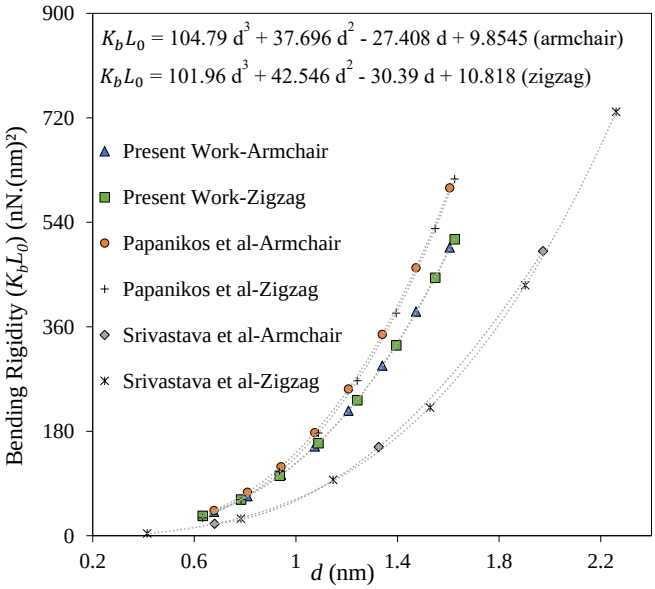

Figure 3: Bending rigidity vs diameter for armchair and zigzag CNTs - A comparison with the literature [113], [114]

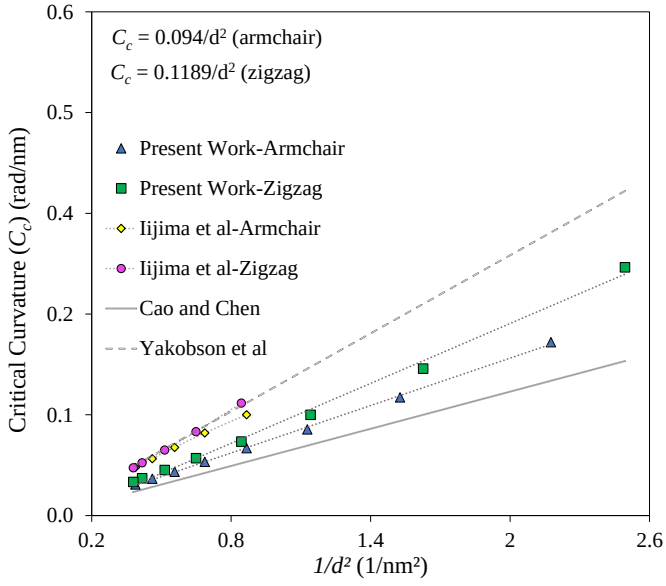

Figure 4: Critical curvature vs diameter for armchair and zigzag CNTs - A comparison with literature [102], [103], [115]

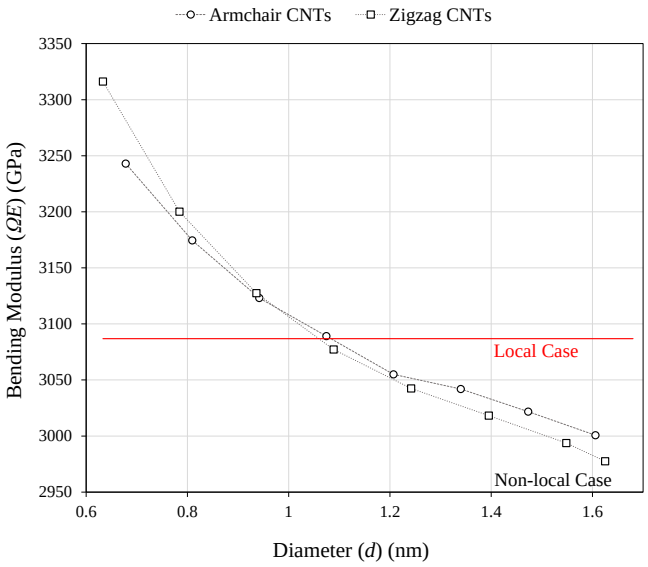

Figure 5: Variation of bending modulus with respect to mean diameter for armchair and zigzag CNTs, and a typical prediction of Cauchy theory

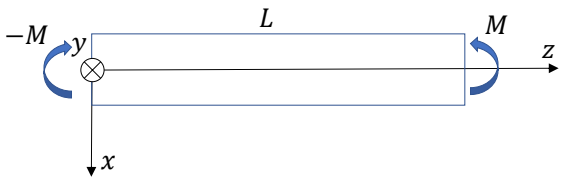

Figure 6: Schematic of the beam under pure bending

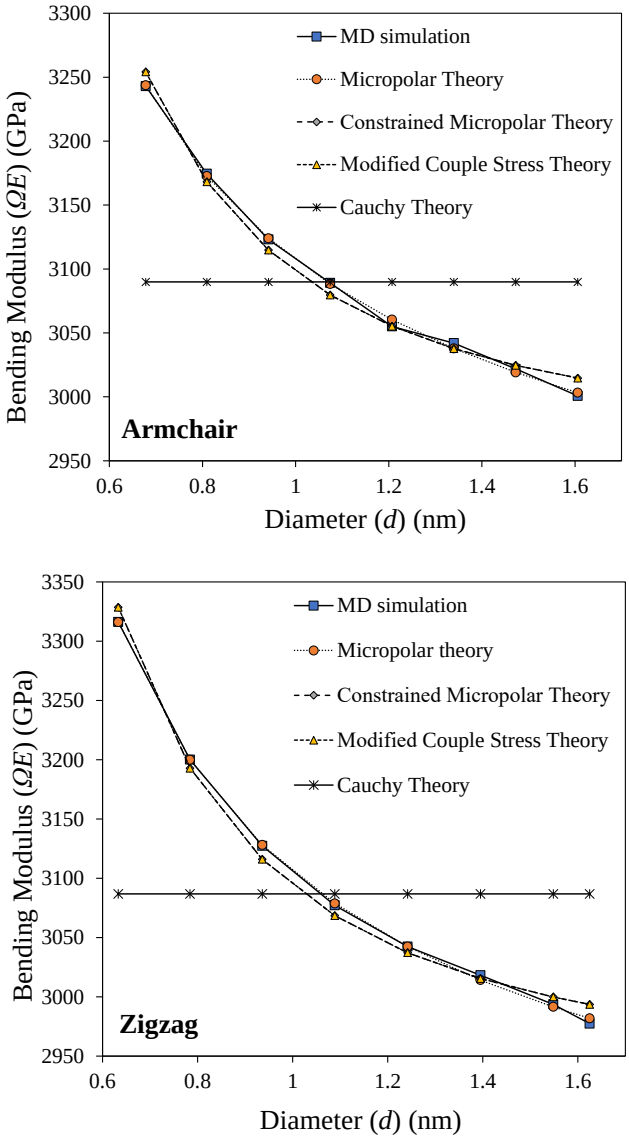

Figure 7: Comparison of the bending modulus of CNTs obtained from MD simulation and different continuum models

Figures Captions:

Figure 1: Schematic of the rotation angle (α), radius of curvature (ρ) and end-to-end distance (l) at the beginning and end of an increment during pure bending, illustrated for an armchair single-walled carbon nanotube with a chirality of $(m, n) = (5, 5)$ and aspect ratio of $L_0/d = 12$ (The changes are exaggerated)

Figure 2: Plots of applied moment of single-walled carbon nanotube with a chirality of $(m, n) = (6, 6)$ and aspect ratio of $L_0/d = 5$ alongside with corresponding buckling mode shapes

Figure 3: Bending rigidity vs diameter for armchair and zigzag CNTs - A comparison with the literature [113], [114]

Figure 4: Critical curvature vs diameter for armchair and zigzag CNTs - A comparison with literature [102], [103], [115]

Figure 5: Variation of bending modulus with respect to mean diameter for armchair and zigzag CNTs, and a typical prediction of Cauchy theory

Figure 6: Schematic of the beam under pure bending

Figure 7: Comparison of the bending modulus of CNTs obtained from MD simulation and different continuum models

References

[1] S. Iijima, "Helical microtubules of graphitic carbon," *Nature*, vol. 354, pp. 56–58, 1991.

[2] S. Iijima and T. Ichihashi, "Single-shell carbon nanotubes of 1-nm diameter," *Nature*, vol. 363, pp. 603–605, 1993.

[3] S. Chopra, K. McGuire, N. Gothard, A. Rao, and A. Pham, "Selective gas detection using a carbon nanotube sensor," *Appl. Phys. Lett.*, vol. 83, no. 11, pp. 2280–2282, 2003.

[4] A. Fennimore, T. Yuzvinsky, W.-Q. Han, M. Fuhrer, J. Cumings, and A. Zettl, "Rotational actuators based on carbon nanotubes," *Nature*, vol. 424, pp. 408–410, 2003.

[5] Y. Yun, V. Shanov, Y. Tu, M. J. Schulz, S. Yarmolenko, S. Neralla, J. Sankar, and S. Subramaniam, "A multi-wall carbon nanotube tower electrochemical actuator," *Nano Lett.*, vol. 6, pp. 689–693, 2006.

[6] P. Williams, S. Papadakis, A. Patel, M. Falvo, S. Washburn, and R. Superfine, "Fabrication of nanometer-scale mechanical devices incorporating individual multiwalled carbon nanotubes as torsional springs," *Appl. Phys. Lett.*, vol. 82, pp. 805–807, 2003.

[7] S. Papadakis, A. Hall, P. Williams, L. Vicci, M. Falvo, R. Superfine, and S. Washburn, "Resonant oscillators with carbon-nanotube torsion springs," *Phys. Rev. Lett.*, vol. 93, p. 146101, 2004.

[8] Y. Zhang, L. F. Duan, Y. Zhang, J. Wang, H. Geng, and Q. Zhang, "Advances in conceptual electronic nanodevices based on 0d and 1d nanomaterials," *Nanomicro Lett.*, vol. 6, pp. 1–19, 2014.

[9] R. Andrews and M. Weisenberger, "Carbon nanotube polymer composites," *Curr. Opin. Solid State Mater. Sci.*, vol. 8, pp. 31–37, 2004.

[10] M. Moniruzzaman and K. I. Winey, "Polymer nanocomposites containing carbon nanotubes," *Macromolecules*, vol. 39, pp. 5194–5205, 2006.

[11] W. Wang and N. Murthy, "Characterization of Nanotube-Reinforced Polymer Composites," in *Carbon Nanotubes*, ch. 8, Rijeka: IntechOpen, 2011.

[12] R. Rafiee, *Carbon Nanotube-Reinforced Polymers: From Nanoscale to Macroscale*. Micro and Nano Technologies, Elsevier Science, 2017.

[13] C. V. Nguyen, K.-J. Chao, R. M. Stevens, L. Delzeit, A. Cassell, J. Han, and M. Meyyappan, "Carbon nanotube tip probes: stability and lateral resolution in scanning probe microscopy and application to surface science in semiconductors," *Nanotechnology*, vol. 12, no. 3, p. 363, 2001.

[14] J.-H. Lee, W.-S. Kang, B.-S. Choi, S.-W. Choi, and J.-H. Kim, "Fabrication of carbon nanotube afm probes using the langmuir–blodgett technique," *Ultramicroscopy*, vol. 108, no. 10, pp. 1163–1167, 2008.

[15] R. M. Stevens, "New carbon nanotube afm probe technology," *Materials today*, vol. 12, no. 10, pp. 42–45, 2009.

[16] H.-C. Liu, D. Fong, G. A. Dahlen, M. Osborn, S. Hand, and J. R. Osborne, "Carbon nanotube afm probes for microlithography process control," in *Metrology, Inspection, and Process Control for Microlithography XX*, vol. 6152, p. 61522Y, International Society for Optics and Photonics, 2006.

[17] B. I. Yakobson and R. E. Smalley, "Fullerene nanotubes: C 1,000,000 and beyond: Some unusual new molecules—long, hollow fibers with tantalizing electronic and mechanical properties—have joined diamonds and graphite in the carbon family," *Am. Sci.*, vol. 85, pp. 324–337, 1997.

[18] V. N. Popov, "Carbon nanotubes: properties and application," *Mater. Sci. Eng. R Rep.*, vol. 43, pp. 61–102, 2004.

[19] J.-P. Salvetat, J.-M. Bonard, N. Thomson, A. Kulik, L. Forro, W. Benoit, and L. Zuppiroli, "Mechanical properties of carbon nanotubes," *Appl. Phys. A*, vol. 69, pp. 255–260, 1999.

[20] M. S. Dresselhaus, G. Dresselhaus, P. Eklund, and A. Rao, "Carbon Nanotubes," in *The Physics of Fullerene-based and Fullerene-related Materials*, pp. 331–379, Springer, 2000.

[21] K. Liew, X. He, and C. Wong, "On the study of elastic and plastic properties of multi-walled carbon nanotubes under axial tension using molecular dynamics simulation," *Acta Mater.*, vol. 52, no. 9, pp. 2521–2527, 2004.

[22] Z. Yao, C.-C. Zhu, M. Cheng, and J. Liu, "Mechanical properties of carbon nanotube by molecular dynamics simulation," *Comput. Mater. Sci.*, vol. 22, no. 3-4, pp. 180–184, 2001.

[23] S. A. Eftekhari, D. Toghraie, M. Hekmatifar, and R. Sabetvand, "Mechanical and thermal stability of armchair and zig-zag carbon sheets using classical md simulation with tersoff potential," *Physica E Low Dimens. Syst. Nanostruct.*, vol. 133, p. 114789, 2021.

[24] R. Izadi, E. Ghavanloo, and A. Nayebi, "Elastic properties of polymer composites reinforced with c60 fullerene and carbon onion: Molecular dynamics simulation," *Physica B Condens. Matter*, vol. 574, p. 311636, 2019.

[25] E. Ghavanloo, R. Izadi, and A. Nayebi, "Computational modeling of the effective young's modulus values of fullerene molecules: a combined molecular dynamics simulation and continuum shell model," *J. Mol. Model.*, vol. 24, no. 3, pp. 1–7, 2018.

[26] R. Izadi, A. Nayebi, and E. Ghavanloo, "Molecular dynamics simulations of structural instability of fullerene family under tension force," *Mol. Simul.*, vol. 44, no. 16, pp. 1338–1343, 2018.

[27] G. Giannopoulos, A. Tsiros, and S. Georgantzinos, "Prediction of elastic mechanical behavior and stability of single-walled carbon nanotubes using bar elements," *Mechanics of Advanced Materials and Structures*, vol. 20, no. 9, pp. 730–741, 2013.

[28] M. Meo and M. Rossi, "Prediction of young's modulus of single wall carbon nanotubes by molecular-mechanics based finite element modelling," *Composites Science and Technology*, vol. 66, no. 11-12, pp. 1597–1605, 2006.

[29] S. K. Georgantzinos and G. I. Giannopoulos, "Thermomechanical buckling of single walled carbon nanotubes by a structural mechanics method," *Diamond and Related Materials*, vol. 80, pp. 27–37, 2017.

[30] M. Rahmandoust and A. Öchsner, "On finite element modeling of single-and multi-walled carbon nanotubes," *Journal of nanoscience and nanotechnology*, vol. 12, no. 10, pp. 8129–8136, 2012.

[31] D. Rapaport, *The Art of Molecular Dynamics Simulation*. Cambridge University Press, 2 ed., 2004.

[32] R. S. Ruoff, D. Qian, and W. K. Liu, "Mechanical properties of carbon nanotubes: theoretical predictions and experimental measurements," *Comptes Rendus Physique*, vol. 4, no. 9, pp. 993–1008, 2003.

[33] K. Dilrukshi, M. Dewapriya, and U. Puswewala, "Size dependency and potential field influence on deriving mechanical properties of carbon nanotubes using molecular dynamics," *Theor. Appl. Mech. Lett.*, vol. 5, no. 4, pp. 167–172, 2015.

[34] P. Trovalusci, "Molecular Approaches for Multifield Continua: Origins and Current Developments," in *Multiscale Modeling of Complex Materials*, pp. 211–278, Springer, 2014.

[35] P. Trovalusci, D. Capecchi, and G. Ruta, "Genesis of the multiscale approach for materials with microstructure," *Arch. Appl. Mech.*, vol. 79, no. 11, pp. 981–997, 2009.

[36] R. Izadi, A. Nayebi, and E. Ghavanloo, "Combined molecular dynamics–micromechanics methods to predict young's modulus of fullerene-reinforced polymer composites," *Eur. Phys. J. Plus*, vol. 136, no. 8, pp. 1–15, 2021.

[37] E. Ghavanloo, H. Rafii-Tabar, and S. A. Fazelzadeh, *Computational Continuum Mechanics of Nanoscopic Structures*. Springer, 2019.

[38] C.-H. Kiang, M. Endo, P. Ajayan, G. Dresselhaus, and M. Dresselhaus, "Size effects in carbon nanotubes," *Phys. Rev. Lett.*, vol. 81, no. 9, p. 1869, 1998.

[39] S. Xiao and W. Hou, "Studies of size effects on carbon nanotubes' mechanical properties by using different potential functions," *Fuller. Nanotub. Carbon Nanostructures*, vol. 14, no. 1, pp. 9–16, 2006.

[40] V. Vijayaraghavan and C. Wong, "Temperature, defect and size effect on the elastic properties of imperfectly straight carbon nanotubes by using molecular dynamics simulation," *Comput. Mater. Sci.*, vol. 71, pp. 184–191, 2013.

[41] M. A. Khorshidi, "Validation of weakening effect in modified couple stress theory: dispersion analysis of carbon nanotubes," *Int. J. Mech. Sci.*, vol. 170, p. 105358, 2020.

[42] M. M. S. Fakhrabadi, A. Rastgoo, M. T. Ahmadian, and M. M. Mashhadi, "Dynamic analysis of carbon nanotubes under electrostatic actuation using modified couple stress theory," *Acta Mech.*, vol. 225, no. 6, pp. 1523–1535, 2014.

[43] R. D. Mindlin, "Micro-structure in linear elasticity," *Arch. Ration. Mech. Anal.*, vol. 16, pp. 51–78, 1964.

[44] I. A. Kunin, "The Theory of Elastic Media with Microstructure and the Theory of Dislocations," in *Mechanics of Generalized Continua* (E. Kröner, ed.), pp. 321–329, Springer Berlin Heidelberg, 1968.

[45] G. Capriz, *Continua with Microstructure*. Springer Tracts in Natural Philosophy, Springer-Verlag, 1989.

[46] M. Gurtin, *Configurational Forces as Basis Concept of Continuum Physics*. Springer-Verlag, 1999.

[47] A. Eringen, *Microcontinuum Field Theory*. Springer, 1999.

[48] A. C. Eringen, *Nonlocal Continuum Field Theories*. Springer Science & Business Media, 2002.

[49] I. Kunin, "On foundations of the theory of elastic media with microstructure," *Int. J. Eng. Sci.*, vol. 22, pp. 969 – 978, 1984.

[50] G. Maugin, *Material Inhomogeneities in Elasticity*. Applied Mathematics, Taylor & Francis, 1993.

[51] M. Tuna and P. Trovalusci, "Stress distribution around an elliptic hole in a plate with 'implicit'and 'explicit'non-local models," *Compos. Struct.*, vol. 256, p. 113003, 2021.

[52] M. Tuna, L. Leonetti, P. Trovalusci, and M. Kirca, "'explicit'and 'implicit'nonlocal continuum descriptions: Plate with circular hole," *Size-Dependent Continuum Mechanics Approaches: Theory and Applications*, p. 311, 2021.

[53] M. Tuna, L. Leonetti, P. Trovalusci, and M. Kirca, "'explicit'and 'implicit'nonlocal continuous descriptions for a plate with circular inclusion in tension," *Meccanica*, vol. 55, no. 4, pp. 927–944, 2020.

[54] M. Tuna and P. Trovalusci, "Scale dependent continuum approaches for discontinuous assemblies:'explicit'and 'implicit'non-local models," *Mech. Res. Commun.*, vol. 103, p. 103461, 2020.

[55] A. Eringen and D. Edelen, "On nonlocal elasticity," *Int. J. Eng. Sci.*, vol. 10, pp. 233 – 248, 1972.

[56] M. Tuna, M. Kirca, and P. Trovalusci, "Deformation of atomic models and their equivalent continuum counterparts using eringen's two-phase local/nonlocal model," *Mech. Res. Commun.*, vol. 97, pp. 26–32, 2019.

[57] A. C. Eringen, "Linear theory of micropolar elasticity," *J. Appl. Math. Mech.*, pp. 909–923, 1966.

[58] W. Nowacki, *Theory of micropolar elasticity*. Springer Verlag, 1970.

[59] P. Trovalusci and A. Pau, "Derivation of microstructured continua from lattice systems via principle of virtual works: the case of masonry-like materials as micropolar, second gradient and classical continua," *Acta Mech.*, vol. 225, pp. 157–177, 2014.

[60] L. Leonetti, F. Greco, P. Trovalusci, R. Luciano, and R. Masiani, "A multiscale damage analysis of periodic composites using a couple-stress/Cauchy multidomain model: Application to masonry structures," *Compos. B. Eng.*, vol. 141, pp. 50–59, 2018.

[61] N. Fantuzzi, P. Trovalusci, and S. Dharasura, "Mechanical behavior of anisotropic composite materials as micropolar continua," *Front. Mater. Sci.*, vol. 6, p. 59, 2019.

[62] P. Trovalusci and G. Augusti, "A continuum model with microstructure for materials with flaws and inclusions," *J. phys., IV*, vol. 8, no. PR8, pp. Pr8–383, 1998.

[63] P. M. Mariano and P. Trovalusci, "Constitutive relations for elastic microcracked bodies: from a lattice model to a multifield continuum description," *Int. J. Damage Mech.*, vol. 8, no. 2, pp. 153–173, 1999.

[64] A. Pau and P. Trovalusci, "A multifield continuum model for the description of the response of microporous/microcracked composite materials," *Mech. Mater.*, p. 103965, 2021.

[65] M. Colatosti, N. Fantuzzi, and P. Trovalusci, "Dynamic characterization of microstructured materials made of hexagonal-shape particles with elastic interfaces," *Nanomaterials*, vol. 11, no. 7, 2021.

[66] N. Fantuzzi, P. Trovalusci, and R. Luciano, "Material symmetries in homogenized hexagonal-shaped composites as Cosserat continua," *Symmetry*, vol. 22, p. 441, 2020.

[67] D. Capecchi, G. Ruta, and P. Trovalusci, "Voigt and Poincaré's mechanistic–energetic approaches to linear elasticity and suggestions for multiscale modelling," *Arch. Appl. Mech.*, vol. 81, pp. 1573–1584, 2011.

[68] V. Sansalone, P. Trovalusci, and F. Cleri, "Multiscale modeling of materials by a multifield approach: Microscopic stress and strain distribution in fiber–matrix composites," *Acta Mater.*, vol. 54, no. 13, pp. 3485–3492, 2006.

[69] M. Pingaro, E. Reccia, P. Trovalusci, and R. Masiani, "Fast statistical homogenization procedure (fshp) for particle random composites using virtual element method," *Comput. Mech.*, vol. 64, no. 1, pp. 197–210, 2019.

[70] P. Trovalusci, M. L. De Bellis, and M. Ostoja-Starzewski, "A statistically-based homogenization approach for particle random composites as micropolar continua," in *Generalized Continua as Models for Classical and Advanced Materials*, pp. 425–441, Springer, 2016.

[71] R. Toupin, "Elastic materials with couple-stresses," *Arch. Rational Mech. Anal.*, vol. 11, no. 1, pp. 385–414, 1962.

[72] R. Mindlin and H. Tiersten, "Effects of couple-stresses in linear elasticity," *Arch. Rational Mech. Anal.*, vol. 11, pp. 415–448, 1962.

[73] W. Koiter, "Couple-stresses in the theory of elasticity, i & ii," 1969.

[74] M. Sokolowski, *Theory of Couple-Stresses in Bodies with Constrained Rotations*. No. 26 in CISM International Centre for Mechanical Sciences, Springer, 1970.

[75] P. Trovalusci and R. Masiani, "Material symmetries of micropolar continua equivalent to lattices," *Int. J. Solids Struct.*, vol. 36, pp. 2091 – 2108, 1999.

[76] A. R. Hadjesfandiari and G. F. Dargush, "Couple Stress theory for solids," *Int. J. Solids Struct.*, vol. 48, pp. 2496–2510, 2011.

[77] A. R. Hadjesfandiari and G. F. Dargush, "An assessment of couple stress theories," 2018.

[78] F. Yang, A. Chong, D. C. C. Lam, and P. Tong, "Couple stress based strain gradient theory for elasticity," *Int. J. Solids Struct.*, vol. 39, pp. 2731–2743, 2002.

[79] H. Ma, X.-L. Gao, and J. Reddy, "A microstructure-dependent timoshenko beam model based on a modified couple stress theory," *J. Mech. Phys. Solids*, vol. 56, no. 12, pp. 3379–3391, 2008.

[80] E. Jomehzadeh, H. Noori, and A. Saidi, "The size-dependent vibration analysis of micro-plates based on a modified couple stress theory," *Physica E Low Dimens. Syst. Nanostruct.*, vol. 43, no. 4, pp. 877–883, 2011.

[81] E. M. Miandoab, H. N. Pishkenari, A. Yousefi-Koma, and H. Hoorzad, "Polysilicon nano-beam model based on modified couple stress and eringen's nonlocal elasticity theories," *Physica E Low Dimens. Syst. Nanostruct.*, vol. 63, pp. 223–228, 2014.

[82] F. Khajueenejad and J. Ghanbari, "Internal length parameter and buckling analysis of carbon nanotubes using modified couple stress theory and Timoshenko beam model," *Mater. Res. Express*, vol. 2, p. 105009, 2015.

[83] B. Akgöz and Ö. Civalek, "Buckling analysis of cantilever carbon nanotubes using the strain gradient elasticity and modified couple stress theories," *J. Comput. Theor. Nanosci.*, vol. 8, pp. 1821–1827, 2011.

[84] Y. Y. Zhang, C. M. Wang, W. Duan, Y. Xiang, and Z. Zong, "Assessment of continuum mechanics models in predicting buckling strains of single-walled carbon nanotubes," *Nanotechnology*, vol. 20, no. 39, p. 395707, 2009.

[85] Q. Wang, "Effective in-plane stiffness and bending rigidity of armchair and zigzag carbon nanotubes," *Int. J. Solids Struct.*, vol. 41, no. 20, pp. 5451–5461, 2004.

[86] I. Arias and M. Arroyo, "Size-dependent nonlinear elastic scaling of multiwalled carbon nanotubes," *Physical review letters*, vol. 100, no. 8, p. 085503, 2008.

[87] H. Farokhi, M. P. Païdoussis, and A. K. Misra, "A new nonlinear model for analyzing the behaviour of carbon nanotube-based resonators," *J. Sound Vib.*, vol. 378, pp. 56–75, 2016.

[88] Q. Wang, "Wave propagation in carbon nanotubes via nonlocal continuum mechanics," *Journal of Applied physics*, vol. 98, no. 12, p. 124301, 2005.

[89] M. Shaat and A. Abdelkefi, "Reporting the sensitivities and resolutions of cnt-based resonators for mass sensing," *Materials & Design*, vol. 114, pp. 591–598, 2017.

[90] Y.-G. Hu, K. M. Liew, Q. Wang, X. He, and B. Yakobson, "Nonlocal shell model for elastic wave propagation in single-and double-walled carbon nanotubes," *Journal of the Mechanics and Physics of Solids*, vol. 56, no. 12, pp. 3475–3485, 2008.

[91] B. Arash and Q. Wang, "A review on the application of nonlocal elastic models in modeling of carbon nanotubes and graphenes," *Computational materials science*, vol. 51, no. 1, pp. 303–313, 2012.

[92] Y. Zhang, G. Liu, and J. Wang, "Small-scale effects on buckling of multiwalled carbon nanotubes under axial compression," *Phys. Rev. B*, vol. 70, p. 205430, 2004.

[93] Y. Zhang, G. Liu, and X. Han, "Effect of small length scale on elastic buckling of multi-walled carbon nanotubes under radial pressure," *Phys. Lett. A*, vol. 349, pp. 370–376, 2006.

[94] F. Khademolhosseini, R. Rajapakse, and A. Nojeh, "Torsional buckling of carbon nanotubes based on nonlocal elasticity shell models," *Comput. Mater. Sci.*, vol. 48, pp. 736–742, 2010.

[95] H.-S. Shen and C.-L. Zhang, "Torsional buckling and postbuckling of double-walled carbon nanotubes by nonlocal shear deformable shell model," *Compos. Struct.*, vol. 92, pp. 1073–1084, 2010.

[96] R. Ansari, H. Rouhi, and S. Sahmani, "Calibration of the analytical nonlocal shell model for vibrations of double-walled carbon nanotubes with arbitrary boundary conditions using molecular dynamics," *Int. J. Mech. Sci.*, vol. 53, pp. 786–792, 2011.

[97] M. Tuna and M. Kırca, "Unification of Eringen's nonlocal parameter through an optimization-based approach," *Mech. Adv. Mater. Struct.*, pp. 1–10, 2019.

[98] G. Xie and S. Long, "Elastic vibration behaviors oof carbon nanotubes based on micropolar mechanics," *Comput. Mater. Contin.*, vol. 4, p. 11, 2006.

[99] L. Wang and H. Hu, "Flexural wave propagation in single-walled carbon nanotubes," *Phys. Rev. B.*, vol. 71, no. 19, p. 195412, 2005.

[100] R. Izadi, M. Tuna, P. Trovalusci, and E. Ghavanloo, "Torsional characteristics of carbon nanotubes: Micropolar elasticity models and molecular dynamics simulation," *Nanomaterials*, vol. 11, no. 2, p. 453, 2021.

[101] T. Chang and J. Hou, "Molecular dynamics simulations on buckling of multiwalled carbon nanotubes under bending," *J. Appl. Phys.*, vol. 100, no. 11, p. 114327, 2006.

[102] S. Iijima, C. Brabec, A. Maiti, and J. Bernholc, "Structural flexibility of carbon nanotubes," *J. Chem. Phys.*, vol. 104, no. 5, pp. 2089–2092, 1996.

[103] G. Cao and X. Chen, "Buckling of single-walled carbon nanotubes upon bending: Molecular dynamics simulations and finite element method," *Phys. Rev. B*, vol. 73, no. 15, p. 155435, 2006.

[104] A. Kutana and K. Giapis, "Transient deformation regime in bending of single-walled carbon nanotubes," *Phys. Rev. Lett.*, vol. 97, no. 24, p. 245501, 2006.

[105] I. A. Nikiforov, *A study of bending deformations in carbon nanotubes using the objective molecular dynamics method.* Thesis, 2010.

[106] P. Poncharal, Z. Wang, D. Ugarte, and W. A. De Heer, "Electrostatic deflections and electromechanical resonances of carbon nanotubes," *science*, vol. 283, no. 5407, pp. 1513–1516, 1999.

[107] R. Lakes, "Experimental Methods for Study of Cosserat Elastic Solids and Other Generalized Elastic Continua," in *Continuum Models for Materials with Microstructure* (H. Muhlhaus, ed.), pp. 1–22, New York: Wiley, 1995.

[108] N. Hamada, S.-i. Sawada, and A. Oshiyama, "New one-dimensional conductors: Graphitic microtubules," *Phys. Rev. Lett.*, vol. 68, pp. 1579–1581, 1992.

[109] S. Plimpton, "Fast parallel algorithms for short-range molecular dynamics," *J. Comput. Phys.*, vol. 117, pp. 1–19, 1996.

[110] W. Humphrey, A. Dalke, and K. Schulten, "Vmd - Visual Molecular Dynamics," *J. Mol. Graph.*, vol. 14, pp. 33–38, 1996.

[111] S. Stuart, A. Tutein, and J. Harrison, "A reactive potential for hydrocarbons with intermolecular interactions," *J. Chem. Phys.*, vol. 112, pp. 6472–6486, 2000.

[112] S. Georgantzinos, G. Giannopoulos, and N. Anifantis, "On the coupling of axial and shear deformations of single-walled carbon nanotubes and graphene: a numerical study," *Proceedings of the Institution of Mechanical Engineers, Part N: Journal of Nanoengineering and Nanosystems*, vol. 224, no. 4, pp. 163–172, 2010.

[113] D. Srivastava and, C. Wei, and K. Cho, "Nanomechanics of carbon nanotubes and composites," *Appl. Mech. Rev.*, vol. 56, no. 2, pp. 215–230, 2003.

[114] P. Papanikos, D. Nikolopoulos, and K. Tserpes, "Equivalent beams for carbon nanotubes," *Comput. Mater. Sci.*, vol. 43, no. 2, pp. 345–352, 2008.

[115] B. I. Yakobson, C. Brabec, and J. Bernholc, "Nanomechanics of carbon tubes: instabilities beyond linear response," *Phys. Rev. Lett.*, vol. 76, no. 14, p. 2511, 1996.

[116] G. Krishna Reddy and N. Venkatasubramanian, "On the flexural rigidity of a micropolar elastic circular cylinder," 1978.

[117] R. Gauthier and W. Jahsman, "A quest for micropolar elastic constants," *J. Appl. Mech.*, vol. 42, pp. 369–374, 1975.

[118] K. M. Liew, Y. Jianwei, and L.-W. Zhang, *Mechanical Behaviors of Carbon Nanotubes: Theoretical and Numerical Approaches*. William Andrew, 2016.

[119] K. N. Kudin, G. E. Scuseria, and B. I. Yakobson, "C 2 f, bn, and c nanoshell elasticity from ab initio computations," *Phys. Rev. B*, vol. 64, p. 235406, 2001.

[120] E. Hernandez, C. Goze, P. Bernier, and A. Rubio, "Elastic properties of c and b x c y n z composite nanotubes," *Phys. Rev. Lett.*, vol. 80, no. 20, p. 4502, 1998.

[121] J. P. Lu, "Elastic properties of carbon nanotubes and nanoropes," *Phys. Rev. Lett.*, vol. 79, no. 7, p. 1297, 1997.

[122] G. K. Reddy and N. Venkatasubramanian, "On the flexural rigidity of a micropolar elastic circular cylindrical tube," *Int. J. Eng. Sci.*, vol. 17, no. 9, pp. 1015–1021, 1979.

[123] A. Taliercio, "Torsion of micropolar hollow circular cylinders," *Mech. Res. Commun.*, vol. 37, pp. 406–411, 2010.

[124] D. Iesan, "Bending of a micropolar elastic beam by terminal couples," *Mathematica*, vol. 17, pp. 483–490, 1979.

[125] F. Beer, R. Johnston, J. DeWolf, and D. Mazurek, *Mechanics of Materials-8th Edition*. McGraw-Hill Education, 2020.

[126] Z. Rueger and R. S. Lakes, "Experimental cosserat elasticity in open-cell polymer foam," *Philosophical Magazine*, vol. 96, no. 2, pp. 93–111, 2016.

[127] R. Lakes and W. Drugan, "Bending of a cosserat elastic bar of square cross section: Theory and experiment," *J. Appl. Mech.*, vol. 82, no. 9, 2015.

[128] Z. Rueger, D. Li, and R. Lakes, "Observation of cosserat elastic effects in a tetragonal negative poisson's ratio lattice," *Phys. Status Solidi B*, vol. 254, no. 12, p. 1600840, 2017.

[129] M. Dunn and M. Wheel, "Size effect anomalies in the behaviour of loaded 3d mechanical metamaterials," *Philosophical Magazine*, vol. 100, no. 2, pp. 139–156, 2020.

[130] A. J. Beveridge, M. Wheel, and D. Nash, "The micropolar elastic behaviour of model macroscopically heterogeneous materials," *Int. J. Solids Struct.*, vol. 50, no. 1, pp. 246–255, 2013.

[131] F.-Y. Huang, B.-H. Yan, J.-L. Yan, and D.-U. Yang, "Bending analysis of micropolar elastic beam using a 3-d finite element method," *Int. J. Eng. Sci.*, vol. 38, no. 3, pp. 275–286, 2000.

[132] B. Hassanati and M. Wheel, "Size effects on free vibration of heterogeneous beams," in *MATEC Web of Conferences*, vol. 148, 2018.

[133] B. Chiu and J. D. Lee, "On the plane problem in micropolar elasticity," *Int. J. Eng. Sci.*, vol. 11, no. 9, pp. 997–1012, 1973.

[134] MATLAB, *version 9.8.0 (R2020a)*. Natick, Massachusetts: The MathWorks Inc., 2020.

[135] T. Vodenitcharova and L. Zhang, "Effective wall thickness of a single-walled carbon nanotube," *Phys. Rev. B*, vol. 68, p. 165401, 2003.

[136] H. W. Kuhn and A. W. Tucker, "Nonlinear Programming," in *Traces and Emergence of Nonlinear Programming*, pp. 247–258, Springer, 2014.

[137] M. Akbarzadeh Khorshidi and D. Soltani, "Nanostructure-dependent dispersion of carbon nanostructures: New insights into the modified couple stress theory," *Math. Methods Appl. Sci.*, 2020.

[138] W. Duan, C. M. Wang, and Y. Zhang, "Calibration of nonlocal scaling effect parameter for free vibration of carbon nanotubes by molecular dynamics," *J. Appl. Phys.*, vol. 101, no. 2, p. 024305, 2007.

[139] H. Askes and E. C. Aifantis, "Gradient elasticity in statics and dynamics: an overview of formulations, length scale identification procedures, finite element implementations and new results," *Int. J. Solids Struct.*, vol. 48, no. 13, pp. 1962–1990, 2011.

[140] Y.-G. Hu, K. M. Liew, and Q. Wang, "Nonlocal elastic beam models for flexural wave propagation in double-walled carbon nanotubes," *J. Appl. Phys.*, vol. 106, no. 4, p. 044301, 2009.

[141] B. WenXing, Z. ChangChun, and C. WanZhao, "Simulation of young's modulus of single-walled carbon nanotubes by molecular dynamics," *Physica B Condens. Matter*, vol. 352, no. 1-4, pp. 156–163, 2004.

[142] N. Sakharova, A. Pereira, J. Antunes, C. Brett, and J. Fernandes, "Mechanical characterization of single-walled carbon nanotubes: Numerical simulation study," *Compos. B. Eng.*, vol. 75, pp. 73–85, 2015.

[143] M. Arroyo and T. Belytschko, "Finite crystal elasticity of carbon nanotubes based on the exponential cauchy-born rule," *Phys. Rev. B*, vol. 69, no. 11, p. 115415, 2004.

[144] B. G. Demczyk, Y. M. Wang, J. Cumings, M. Hetman, W. Han, A. Zettl, and R. Ritchie, "Direct mechanical measurement of the tensile strength and elastic modulus of multiwalled carbon nanotubes," *Mater. Sci. Eng. A*, vol. 334, no. 1-2, pp. 173–178, 2002.

[145] J.-P. Salvetat, G. A. D. Briggs, J.-M. Bonard, R. R. Bacsa, A. J. Kulik, T. Stöckli, N. A. Burnham, and L. Forró, "Elastic and shear moduli of single-walled carbon nanotube ropes," *Phys. Rev. Lett.*, vol. 82, no. 5, p. 944, 1999.

[146] M. J. Treacy, T. W. Ebbesen, and J. M. Gibson, "Exceptionally high young's modulus observed for individual carbon nanotubes," *nature*, vol. 381, no. 6584, pp. 678–680, 1996.

[147] A. Krishnan, E. Dujardin, T. Ebbesen, P. Yianilos, and M. Treacy, "Young's modulus of single-walled nanotubes," *Phys. Rev. B*, vol. 58, no. 20, p. 14013, 1998.

[148] E. W. Wong, P. E. Sheehan, and C. M. Lieber, "Nanobeam mechanics: elasticity, strength, and toughness of nanorods and nanotubes," *science*, vol. 277, no. 5334, pp. 1971–1975, 1997.

[149] A. A. Farajian, B. I. Yakobson, H. Mizuseki, and Y. Kawazoe, "Electronic transport through bent carbon nanotubes: nanoelectromechanical sensors and switches," *Phys. Rev. B*, vol. 67, no. 20, p. 205423, 2003.

[150] P. Liu, Y. Zhang, C. Lu, and K. Lam, "Tensile and bending properties of double-walled carbon nanotubes," *J. Phys. D Appl. Phys.*, vol. 37, no. 17, p. 2358, 2004.

6 Appendix

Comparison of the bending method applied in different researches

Author	Simulation Method	Potential	Loading Method	CNT type	Temp. (K)
Chang & Hou [101]	MD	REBO II	A constant increment of bending angle is applied, the loading atoms are fixed and the whole tube is relaxed in NVT ensemble for 50 steps at each increment.	armchair MWCNTs with the same outer tube as (35, 35) and L =12.4 nm	1
Farajian et al. [149]	tight binding	-	While fixing eight carbon rings at each end of the nanotube, the structure is optimized such that the maximum force acting on the unconstrained atoms becomes less than 0.05 eV/Å.	(6,6) and (10,0)	-
Liu et al. [150]	tight binding	REBO	A lateral force is applied to each atom at the loading end. The bending force is the summation of all the applied lateral forces.	(5, 5)/(10, 10)	0
Iijima et al. [102]	MD	Tersoff-Brenner	The bending angle was increased in small steps and the tube was relaxed at each position. The presence of the bending force was simulated by keeping the end atoms fixed for each configuration.	SWCNT of diameters varying between 1.0 nm and 1.5 nm and covering the entire range of helicity	0 & 300
Yakobson et al. [115]	MD	Tersoff-Brenner	In simulations of bending, a torque is applied at the ends, and the bending angle increases stepwise	Same as [102]	50
Kutana and Giapis [104]	MD	REBO and Lennard-Jones	By rotating the fixed ends in steps of 0.5 degree . After each step, the potential energy of the central segment was minimized . The axial strain was removed through a succession of end displacements and central part relaxations.	(10, 10) and (30, 30)	300
Cao and Chen [103]	ab initio and FEM	COMPASS	Rigid body translation is applied to the atoms in both end layers of SWCNT, such that the length of the deformed tube axis remains unchanged. The carbon atoms in both end layers are first moved to and fixed at their new positions, then, all other carbon atoms relocate to their new equilibrium positions by minimizing the potential energy of the whole system.	(5,5), (10,10), (15,15), (20,20), (9,0), (17,0), (26,0) and (35,0)	0
Nikiforov [105]	Objective MD	Tersoff	The bending angle was varied in small steps, at most 0.05 degrees per nm of tube length, with relaxation performed at each step.	SWCNTs with radii ranging from 0.35 nm (5,5) to 1.40 nm	300